J. Physiol. (1983), **335**, *pp.* 393–426
With 10 *text-figures*
Printed in Great Britain

ANALYSIS OF POTASSIUM DYNAMICS IN MAMMALIAN BRAIN TISSUE

BY A. R. GARDNER-MEDWIN
From the Department of Physiology, University College London, London WC1E 6BT

(*Received 12 January 1982*)

SUMMARY

1. Equations are derived for potassium (K^+) dynamics in simplified models of brain tissue. These describe K^+ movement in extracellular space, transfer of K^+ associated with current flow through cells (the so-called spatial buffer mechanism) and equilibration between extracellular space and cytoplasm.

2. Numerical calculations show that the principal data on K^+ dynamics from various laboratories can be accounted for with simple assumptions about spatial buffer action and uptake. Much of the data is inconsistent with extracellular diffusion being the main mechanism for K^+ flux through brain tissue, including some that has earlier been cited in support of this hypothesis.

3. The buffering actions of spatial buffer transfer of K^+ and of cytoplasmic equilibration, in which these mechanisms reduce rises of $[K^+]_o$ that would otherwise occur, are analysed quantitatively for specific K^+ source distributions and for spatial and temporal frequency components of general disturbances.

4. Spatial buffer action has most effect in reducing $[K^+]_o$ rises with net release over extensive zones of tissue (greater than *ca.* 200 μm in diameter) for periods of the order of minutes. Reductions greater than 75% may be achieved. With localized but prolonged release, the maximum $[K^+]_o$ rise is little affected but the volume of tissue affected by more moderate rises is substantially reduced.

5. Cytoplasmic K^+ uptake also has most effect with widespread release, but its effect diminishes with prolonged periods of release.

6. The effects of the buffering mechanisms and of K^+ re-uptake into active neurones in determining the decline of $[K^+]_o$ after a period of stimulation are considered. Re-uptake is unlikely to be the major factor responsible for $[K^+]_o$ decline when this has a time course of only a few seconds.

7. The properties necessary for the cells mediating the spatial buffer mechanisms, possibly glial cells, are assessed.

INTRODUCTION

The aim of this paper is to relate the data on potassium movement through brain tissue to the predictions of some simple models of the tissue. This provides a framework for the quantitative interpretation of data obtained in the preceding two papers (Gardner-Medwin, 1983; Gardner-Medwin & Nicholson, 1983). Using numerical

methods, with a single fairly simple model, it is possible to predict the size and the time course of three different types of data obtained in these papers: measurements of the potassium flux across the tissue surface associated with current flow (Gardner-Medwin, 1983), measurements of the extracellular concentration changes associated with current flow (Gardner-Medwin & Nicholson, 1983) and measurements of the extracellular voltage changes associated with K^+ flux (Gardner-Medwin, 1983). The substantial agreement between the data and these calculations suggests that the various phenomena may result from the same mechanism and that it is not necessary to postulate additional processes to account for the results. This strengthens the conclusions that have already been drawn from simpler arguments within these two papers. These conclusions are that the principal means by which potassium (K^+) moves through vertebrate brain tissue from one region of extracellular space to another is through cells rather than through the extracellular space directly. This applies both to movement in a K^+ concentration gradient and to movement in a voltage gradient, when these gradients extend for distances of several hundred microns.

These conclusions go against the interpretations suggested for other data, particularly the suggestions made by Fisher, Pedley & Prince (1976) and Lux & Neher (1973) for their experiments. The theoretical analysis in this paper can be used to examine these other experiments and to consider the extent to which the different data really entail different conclusions. This discussion highlights some of the questions that remain to be answered about K^+ dynamics in brain tissue.

The importance of K^+ dynamics in neural tissue is described in the Introduction to an accompanying paper (Gardner-Medwin, 1983) and, for example, by Varon & Somjen (1979). One of the major questions is whether there are mechanisms within the brain that specifically limit the build-up of K^+ around active neurones. The analysis in this present paper indicates to what extent and under what conditions the postulated mechanisms would limit the increases of extracellular K^+ concentration with different patterns of release. There are at present no straightforward ways of turning on and off the mechanisms for K^+ uptake into cells and K^+ dispersal in an experiment, to determine their effect, but once we can estimate their parameters we can calculate what the effect of such hypothetical experiments would be.

Some of the conclusions from this analysis have been published in preliminary form (Gardner-Medwin, 1980, 1981*b*).

Principal simplifying assumptions

Vertebrate brain tissue contains many types of cells with differing morphology and physiology. Each cell type may affect the extracellular K^+ concentration ($[K^+]_o$) and the K^+ flux through the tissue in one or more ways. The approach here is to make simplifying assumptions for a model of the tissue, to calculate the expected results with these assumptions, and to see whether there are aspects of the experimental results that cannot be explained on the basis of these assumptions. A reasonable agreement between the experimental results and calculations does not, of course, demonstrate the validity of the assumptions. It does, however, show that further experiments, probably of a different design, would be required to establish if the simplified model is seriously misleading in predicting the tissue behaviour. The assumptions in the model are presented here.

(i) *The nature of the extracellular space.* The extracellular space in all regions of the tissue has, in the model, the same physical parameters, including the extracellular volume fraction (α) and tortuosity factor (λ), defined on p. 402. The tortuosity factor (λ) is assumed to be the same in all directions: i.e. the tissue is isotropic. The mobilities of the principal conducting ions (Na^+, K^+ and Cl^-) and their concentrations under base-line conditions are the same as in cerebrospinal fluid, with K^+ having a base-line transport number (n_B) of 0·012 (Gardner-Medwin, 1983). The movement of ions in the extracellular space under the influence of concentration and electrical gradients obeys the Nernst–Planck equation (eqn (17)), as in a simple aqueous solution. For this and other electrochemical theory the reader should refer to a standard text (e.g. Bockris & Reddy, 1970).

(ii) *The relation between extracellular K^+ concentration and tissue K content.* It is known that a rise in $[K^+]_o$ results in net uptake of K^+ into cytoplasm in at least some tissues (Boyle & Conway, 1941; Lund-Andersen & Hertz, 1970). The time course for equilibration of such uptake into cells in brain tissue is uncertain but is probably rapid (a few seconds) because of the high surface to volume ratio of neurites and glia (Gardner-Medwin, 1980). Most of the important results in the present analysis involve effects with time courses of tens or hundreds of seconds. For these results it is assumed that the local tissue is always fully equilibrated. In experiments with ionophoretic K^+ injection (Lux & Neher, 1973; Nicholson, Phillips & Gardner-Medwin, 1979) the observed changes of $[K^+]_o$ are faster. For such experiments a simple linear differential equation for uptake is included (p. 405).

When $[K^+]_o$ is raised in the tissue for long enough for the local cytoplasmic K^+ concentration to reach a new steady level, the local K^+ content of the tissue is raised by more than just the amount present in the extracellular space. This can be expressed in terms of an effective K^+ distribution space ξ, which is the ratio of the change in tissue K^+ content (m-mole per litre of tissue) to the change in $[K^+]_o$ (mM). If equilibration took place only in extracellular space, ξ would be *ca.* 0·2, i.e. the fraction of the tissue volume that is extracellular space. For mammalian brain slices the data of Lund-Andersen & Hertz (1970, Fig. 3) gives ξ in the range 1·0–1·4, while the classic work of Boyle & Conway (1941) on frog muscle gives ξ *ca.* 0·8. In frog muscle the K^+ uptake was shown by Boyle & Conway to be the same whether it was produced by K/Na substitution in extracellular space (when there was cell swelling) or by KCl addition (when cell volume remained approximately constant and cytoplasmic K^+ concentration was raised). A constant value $\xi = 1{\cdot}0$ is assumed here for brain tissue.

(iii) *The cells that aid K^+ transfer between regions of extracellular space.* These cells embody the simplest properties required for the transfer of extracellular K^+ by the spatial buffer mechanism (Orkand, Nicholls & Kuffler, 1966). The simplifying assumption is made that all the cells that contribute to such transfer have the same electrical parameters and purely K^+-selective membranes. They are referred to here as *transfer cells.* Their properties make them resemble glial cells rather more than neurones. In total they need only occupy a small fraction of the tissue volume: enough for their cytoplasm to carry about 6% of an electric current through the tissue. In line with the assumption that all the K^+ transfer cells can be lumped together, the fraction of tissue current through other cell types is assumed negligible (Fig. 1). This

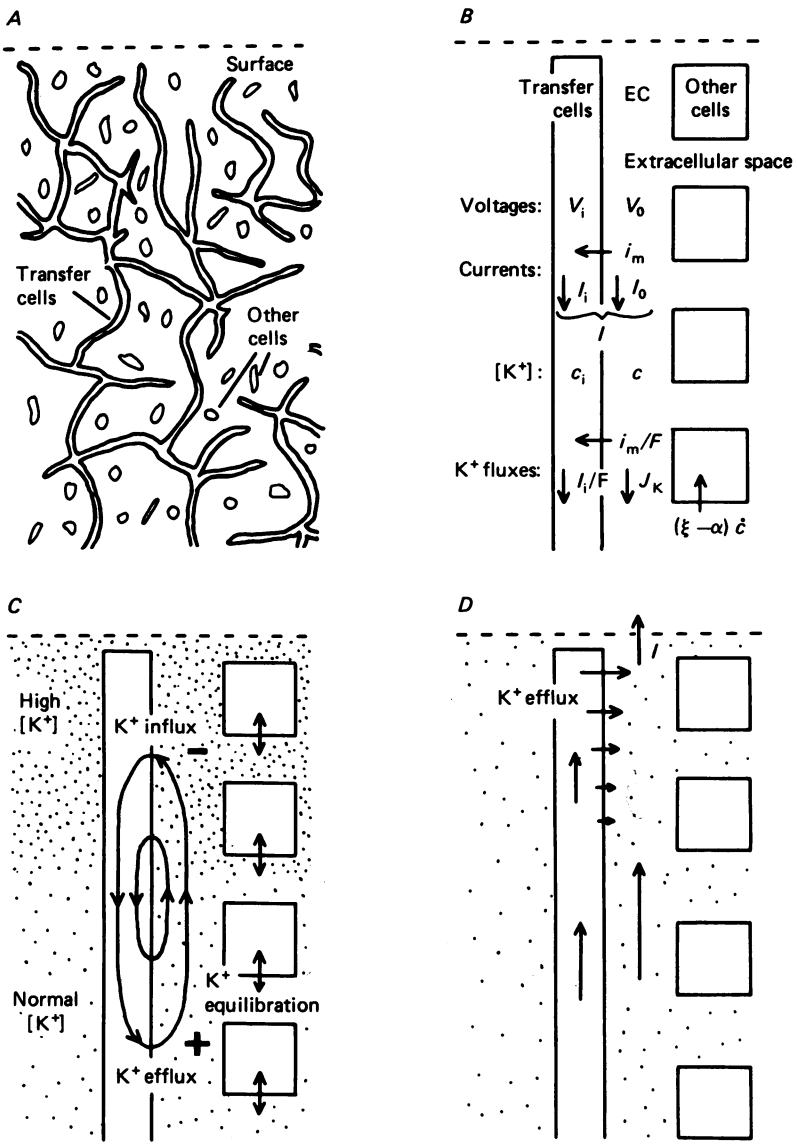

Fig. 1. Schematic diagrams of the tissue. *A*, the network of transfer cell processes assumed to be electrically coupled throughout the tissue and terminated at the surface. Most of the tissue volume is occupied by other cells, of which only a few are indicated. *B*, the principal variables. *C*, the pattern of currents and K^+ fluxes associated with the spatial buffer mechanism in the transfer cells when there is a gradient of extracellular K^+ concentration. *D*, the currents and K^+ efflux from transfer cells when a current is passed outward across the tissue surface.

is consistent with the other cell types (presumably mainly neurones) occupying a majority of the tissue volume if these cells have tortuous or short processes compared with their electrical space constants.

Since the transfer cell membranes are K^+-selective, they have no significant passive or active Na^+ fluxes (see discussion by Gardner-Medwin, 1981*a*, in relation to glial

cells). Their resting potentials are equal to the Nernst equilibrium potential for K^+. The membrane K^+ flux for these cells is related to the membrane potential and to the internal and external K^+ concentrations by the constant field equations (Goldman, 1943). This is an essentially arbitrary choice, in the absence of specific information about the $[K^+]_o$ dependence of membrane conductance for central neurones and glia.

The cytoplasm of adjacent transfer cells is assumed to be coupled in a syncytial manner, allowing passage of current (Fig. 1*A*). The total current flowing through the cytoplasm of transfer cells per unit area of tissue is related to the average gradient of intracellular voltage along the direction of current by a simple resistivity parameter (r_i). This parameter is made up of components due to (*a*) the resistivity and tortuosity of the cytoplasm and (*b*) the resistance of junctions between the cells, as discussed by Somjen (1973). The postulate that the transfer cells form a syncytium is not strictly necessary. Independent transfer cells with processes that overlap with their neighbours by distances much greater than their electrical space constants would behave in essentially the same way. Any component of current passing long distances through a succession of such cells, through cytoplasm and across membranes in the overlapping zones, would encounter the largest electrical resistance in the cytoplasm and would have no net effect on the ionic composition of the extracellular space within each overlap zone. A syncytium is assumed (Fig. 1*A*), simply because it is easier to envisage and discuss.

The K^+ concentration within the transfer cells is assumed to be constant. Changes of the total K^+ content of the transfer cells cannot occur since their membranes do not pass other ions to maintain electroneutrality. Thus it is other cell types in the tissue that contribute the substantial cytoplasmic component of the total K^+ distribution space ((ii), above). Current flow across the transfer cell membranes will not cause intracellular build-up or depletion of K^+ if both the membrane current and the cytoplasmic current are carried entirely by K^+ ions. This assumption is probably approximately correct for vertebrate glial cells (Somjen, 1975, 1979) and represents the simplest form of spatial buffer action that can be included in a model. Spatial buffering may also occur in situations where significant intracellular concentration changes occur in the transfer cells, where these do not have high internal $[K^+]$ (Gardner-Medwin, Coles & Tsacopoulos, 1981).

(iv) *Water movements between compartments of the tissue.* The fluxes of ions between different compartments of the tissue can result in water movements. This, in turn, may affect ion concentrations through changes of the compartment volumes (Gardner-Medwin, 1980). Potassium represents only *ca.* 1 % of the osmotic constituents of extracellular fluid however, so disturbances affecting $[K^+]_o$ directly are associated with proportionately much smaller changes of osmolarity. Such effects are ignored in this simplified analysis, though it must be recognized that in some extreme conditions the concentrations of all extracellular ions may be significantly affected by water movements (Dietzel, Heinemann, Hofmeier & Lux, 1980). The lack of significant extracellular volume changes during current passage experiments is borne out by the failure to observe significant changes of $[Ca^{2+}]_o$ (Gardner-Medwin & Nicholson, 1983).

(v) *Exchange of K^+ with the blood.* In vertebrate brain the ionic permeability of cerebral capillaries is extremely low and consequently it is unlikely that significant effects on concentration within brain tissue due to capillary exchange can be seen

in times less than many tens of minutes (Gardner-Medwin, 1980). Such effects are neglected except in considering the data of Fisher *et al.* (1976), which involves changes of $[K^+]_o$ maintained for several hours (pp. 411–412).

(vi) *The surface of the brain.* The extracellular space is assumed to open straight into the fluid at the pia-arachnoid or ependymal surface of the brain without any form of barrier. The processes of the transfer cells terminate in closed ends at the surface (fig. 2*A*), but are otherwise uniform throughout the entire tissue up to the surface.

Bennett (1969) used an electrical technique to show that careful dissection in the cat could leave a fragile barrier intact at the pia-arachnoid cortical surface (presumably the arachnoid membrane) that had a resistance of 200–400 Ω cm², equivalent to that of 5–10 mm thickness of brain tissue. (Note that figures of 50–100 Ω cm² in the paper are calculated erroneously from the data: M. V. L. Bennett, personal communication.) This membrane could be a substantial barrier for K^+ diffusion. It was absent in the experiments of Gardner-Medwin (1983) and Gardner-Medwin & Nicholson (1983) since voltage profiles during current passage would have revealed an appreciable jump in voltage across the surface with less than a tenth of this resistance. Fisher *et al.* (1976) have suggested that there was a barrier for K^+ diffusion into cat cortex in their experiments. Again, the arachnoid membrane is unlikely to have been intact in these experiments since the suggested barrier is not discretely localized at the surface: an explanation of the apparent barrier as due simply to operation of the spatial buffer mechanism is more likely (pp. 411–412). The assumption that there is no significant extracellular barrier at the pial or ependymal surfaces is consistent with the data of Levin, Fenstermacher & Patlak (1970) for diffusion of extracellular markers from the cerebrospinal fluid into brain tissue.

(vii) *Geometrical simplifications.* The experimental data with current flow across the brain surface and with changes of fluid composition at the brain surface are both compared to one-dimensional solutions of the equations derived below. This comparison would be wholly valid if the cortical surface were entirely flat and uniformly affected by the experimental procedures. In fact it is convex within the area of the experimental cups and will be somewhat differently affected towards the edge of a cup. Errors due to this one-dimensional assumption should be small so long as the results refer only to depths that are much less than the cup diameter (5 mm for the rat neorcortex, 3 mm for the cerebellum). This is normally the case.

Data from experiments with ionophoretic release of K^+ are compared with three-dimensional spherically symmetrical solutions of the equations (p. 404). In order to simplify the nomenclature, the equations are derived for one-dimensional situations (pp. 400–403) and the modifications for radial analysis are described on

MATHEMATICAL DESCRIPTION

Some readers may wish to omit the mathematical analysis (pp. 400–404) and proceed to the Results (p. 406), which should be comprehensible with occasional reference to the Definitions below and the section on the meaning of some of the derived parameters (p. 405).

Definitions

Asterisks (*) indicate tissue parameters that are variables: i.e. that vary with time and/or position in the tissue; the chief variables are shown in Fig. 1*B*. Other parameters are constants in the analysis. Abbreviations are used for partial derivatives with respect to time (t) and distance along the x axis:

$$\dot{Y} = \frac{\partial Y}{\partial t};\ Y' = \frac{\partial Y}{\partial x};\ Y'' = \frac{\partial^2 Y}{\partial x^2}.$$

The symbol Δ before a variable indicates a deviation from its resting level.

Fundamental constants

R Gas constant: 8·32 J K^{-1} $mole^{-1}$
T Absolute temperature: 310 K at 37 °C
F Charge per mole of univalent ions: 96·5 kC/mole
Ψ RT/F: 27 mV at 37 °C
D_{aq} Aqueous diffusion coefficient for K^+ ions: *ca.* $2{\cdot}5 \times 10^{-5}$ cm^2 sec^{-1} at 37 °C, $1{\cdot}9 \times 10^{-5}$ cm^2 sec^{-1} at 20 °C calculated from mobilities given by Conway (1952)

General tissue parameters

α Fraction of total tissue volume occupied by extracellular space
λ Extracellular tortuosity factor (p. 402)
$*c$ Extracellular K^+ concentration ($[K^+]_o$)
c_B Base-line (i.e. normal resting) value of c
n_B Base-line transport number for K^+ in extracellular space: called t_K in Gardner-Medwin (1983)
D Diffusion coefficient for K^+ ions in the extracellular space (p. 402)
ξ Distribution space for K^+ (pp. 395, 405)
τ_{eq} Time constant for equilibration of tissue cytoplasm with altered levels of c (p. 405)
$*V_o$ Electrical potential in extracellular space with respect to remote tissue
$*I_o$ Extracellular current flowing through a tissue plane perpendicular to the x direction, per unit area of tissue
r_o Extracellular tissue resistance (Ω m), equal to V_o'/I_o (p. 400)
$*I$ Total tissue current in the x direction, per unit area of tissue
$*J_K$ Extracellular K flux in the x direction, per unit area of tissue
$*Q$ Rate of release of K^+ into extracellular space, per unit volume of tissue (p. 402)
$*I_R$ Total tissue current through a spherical surface in radial solutions (p. 404)

Parameters of the transfer cells

$*V_i$ Electrical potential in the cytoplasm of transfer cells
$*V_m$ Membrane potential of transfer cells: $V_i - V_o$
V_r V_m under resting (or base-line) conditions
$*i_m$ Net inward ionic current per unit area of transfer cell membrane (p. 400)
R_m Resistance of unit area of transfer cell membrane $(-\partial V_m/\partial i_m)$ under resting conditions
C_m Capacitance of unit area of transfer cell membrane
τ Time constant of transfer cell membrane under resting conditions ($R_m C_m$)
a Area of transfer cell membranes per unit volume of tissue
P Permeability of transfer cell membranes to K^+ (p. 401)
$*I_i$ Current in transfer cell cytoplasm through a plane perpendicular to x, per unit area of tissue
r_i Resistance of the cytoplasm of the transfer cells (Ω m), equal to V_i'/I_i (p. 400)
c_i K^+ concentration within the transfer cells (p. 397)

Combined parameters

Λ $[R_m a^{-1}(r_i + r_o)^{-1}]^{\frac{1}{2}}$: the electrical space constant of the transfer cells within the tissue under resting conditions (p. 405)
T $\xi\lambda^2\Lambda^2\alpha^{-1}D^{-1}$: a characteristic time within the tissue (p. 405)
β $(n_B^{-1} - 1)\, r_o(r_i + r_o)^{-1}$: a measure of the relative magnitude of K^+ flux through the transfer cells and by extracellular diffusion (pp. 405–406).

Cable equations for the transfer cells

Both the membrane potential (V_m) and the ionic current (i_m) across the membranes of the transfer cells may vary throughout the tissue. If there are variations of $[K^+]_o$ (designated by c), then V_m might be expected to follow these variations according to the Nernst equation for K^+, since the membranes are solely permeable to K^+. But this is not precisely correct, since gradients of V_m must be associated with currents flowing through extra- and intracellular space and across the membranes, and these act so that V_m is affected not only by the *local* extracellular K^+ concentration, but also by the regions within a distance of several space constants (Λ). The membrane currents that flow in such a situation act to move K^+ into or out of the extracellular space (Fig. 1*C*) in a pattern that serves to shift K^+ from regions where $[K^+]_o$ is high to regions where it is low. This is known as the spatial buffer mechanism for dispersal of K^+ (Orkand *et al.* 1966). Calculation of the current and voltage distribution associated with a particular distribution of $[K^+]_o$ follows approximately the principles of conventional cable analysis (see e.g. Jack, Noble & Tsien, 1975). In many situations the spatial buffer mechanism operates with zero net current through the tissue ($I = 0$), since extracellular currents in one direction are balanced by intracellular currents in the other direction. The equations are derived for situations in which I is not necessarily zero, since this more general analysis is appropriate for some of the experiments, as well as for certain assymetrical cases of spatial buffering where one region of tissue may drive net current through another region.

A current density I through the tissue in the x direction is the sum of the extra- and intracellular current densities, each expressed per unit area of tissue:

$$I = I_o + I_i. \tag{1}$$

If the current is parallel to x without diverging, we have:

$$I_o' + I_i' = 0. \tag{2}$$

The extracellular component I_o is carried by all the extracellular ions, i.e. largely Na^+ and Cl^-. The intracellular component I_i is a K^+ current flowing entirely within the transfer cells (p. 397). The definitions of the extracellular and intracellular resistance parameters (r_o, r_i) are expressed in the following two equations. Note that these parameters are the resistances of the extra- and intracellular compartments between the faces of a unit cube of tissue. They therefore depend on the geometry of the compartments as well as on the specific resistance of the respective fluids and on the properties of intercellular junctions.

$$V_i' = -r_i I_i, \tag{3}$$

$$V_o' = -r_o I_o. \tag{4}$$

Gradients of ion concentrations in extracellular space can themselves cause voltage gradients (i.e. diffusion potentials) with no net current, through the unequal mobilities of the diffusing ions. These effects are ignored except for Fig. 4*C*, where they are separately estimated for comparison with results from the model. The area of transfer cell membrane in unit volume of tissue is (a) and its specific membrane capacitance is C_m. In regions with an inward current density i_m across the transfer cell membranes (representing a pure K^+ flux) the equation for charging of the membrane capacitance is:

$$aC_m \dot{V}_m = I_o' + ai_m. \tag{5}$$

Using the conventional manipulations of cable theory to operate on eqns. (1)–(5), we derive eqns. (6)–(8):

$$\dot{V}_m = \frac{1}{\tau}[R_m i_m + \Lambda^2 V_m''], \tag{6}$$

$$V_o' = -\frac{r_o}{r_i + r_o}[V_m' + r_i I], \tag{7}$$

$$V_o'' = -\frac{r_o}{r_i + r_o} V_m'', \tag{8}$$

where τ, Λ are the time constant and the electrical space constant for the network of coupled transfer cells under resting conditions (pp. 399, 405). Equation (6) is the conventional cable equation, while

eqns (7)–(8) are subsidiary equations required in later analysis. Provided that C_m, a, r_i and r_o do not vary, these equations are valid even for different K^+ concentrations, in which the membrane resistance will vary. Note that R_m, τ, Λ are not variables: they are the values that the corresponding variables have under resting conditions (p. 399).

The membrane current (i_m) depends on the K^+ concentrations and on V_m in a manner determined by the membrane characteristics. With constant field assumptions (p. 397) and a constant K^+ permeability (P), i_m is given by eqn (9) (see e.g. Jack *et al.* 1975):

$$i_m = -\frac{FP}{\Psi}\frac{V_m[c_i \exp(V_m/\Psi) - c]}{\exp(V_m/\Psi) - 1}. \tag{9}$$

The internal K^+ concentration of the transfer cells (c_i) is assumed not to vary significantly from its resting level (p. 397). Since the membranes are solely permeable to K^+, c_i is related to the base-line $[K^+]_o$ ($= c_B$) and to the resting potential (V_r) by the Nernst equation:

$$c_i = c_B \exp(-V_r/\Psi). \tag{10}$$

This expression is later substituted into eqn (9). It is also convenient to substitute an expression for the membrane permeability (P) as a function of the resting specific membrane resistance (R_m), which is the parameter used in the definitions of τ and Λ. To obtain the resting conductance we can differentiate eqn. (9) with respect to V_m and substitute the resting conditions ($V_m = V_r$; $c = c_B$):

$$\frac{\partial i_m}{\partial V_m} = -R_m^{-1} = -\frac{FP}{\Psi^2}\frac{V_r c_B}{\exp(V_r/\Psi) - 1}. \tag{11}$$

Rearranging eqn. (11) gives:

$$P = \frac{\Psi^2}{R_m F V_r c_B}[\exp(V_r/\Psi) - 1]. \tag{12}$$

Substituting eqns. (10) and (12) into eqn. (9) gives:

$$i_m = \frac{\Psi V_m[\exp(V_r/\Psi) - 1]}{R_m V_r[\exp(V_m/\Psi) - 1]}\left[\frac{c}{c_B} - \exp((V_m - V_r)/\Psi)\right]. \tag{13}$$

This expression for i_m is substituted in eqn (6) to give the full cable equation:

$$\dot{V}_m = \frac{1}{\tau}\left[\Psi\frac{V_m[\exp(V_r/\Psi) - 1]}{V_r[\exp(V_m/\Psi) - 1]}\left[\frac{c}{c_B} - \exp((V_m - V_r)/\Psi)\right] + \Lambda^2 V_m''\right]. \tag{14}$$

A linear approximation to eqn. (14) can be derived that is adequate for many calculations involving small displacements from resting conditions:

$$\dot{V}_m \simeq \frac{1}{\tau}\left[\Psi\frac{c - c_B}{c_B} - (V_m - V_r) + \Lambda^2 V_m''\right]. \tag{15}$$

This linearized form is independent of specific assumptions about the dependence of i_m on V_m or $[K^+]_o$, provided the resting membrane is at K^+ equilibrium. Equation (14) reduces to this form for $|V_m - V_r| \to 0$. With $V_r/\Psi = -3$ (i.e. transfer cell resting potentials *ca.* -80 mV), the errors introduced by the approximation, compared with eqn. (14), are less than 20 % for depolarizations less than 10 mV.

Equation (14) or (15) allows calculation of the rate of change of membrane potential of the transfer cells at every point if the distributions of membrane potential and of $[K^+]_o$ are known. In practice the time constant of the membranes (τ) is so short (a few msec at most) and in the situations of interest the changes of c are so slow ($|\dot{c}| \ll |\Delta c|/\tau$) that the membrane always reaches a pseudo-stationary state indistinguishable from that for which $\tau\dot{V}_m = 0$. The distributions of currents and voltages are the same at every instant as they would be if the prevailing distribution of c were in fact steady. In the numerical calculations the changes of c are obtained with equations derived below and V_m is then calculated after each step by integration of eqn. (14) or (15) to a steady state. An expression for i_m is required later, which follows from eqn. (6) by substituting $\tau\dot{V}_m = 0$:

$$i_m = -\frac{\Lambda^2}{R_m} V_m''. \tag{16}$$

Equations for extracellular potassium flux through the tissue

The flux of K^+ through an aqueous solution depends on the gradients of extracellular voltage and of $[K^+]$ according to the Nernst–Planck equation (see e.g. Bockris & Reddy, 1970). The actual size of the flux J_K in extracellular space (defined as the amount of K^+ moving through the extracellular channels within unit area of tissue per sec) will be smaller than in free solution with the same gradients because of (*a*) the limited extracellular space available, (*b*) the fact that not all of this space is devoted to parallel sided channels going in the direction of the flux. It is convenient to write the factor by which the flux is reduced as $\alpha\lambda^{-2}$ where α is the extracellular space fraction and λ is conventionally known as the tortuosity factor, though it is strictly a geometrical factor that differs from unity both on account of true tortuosity (twistiness) of the extracellular channels and through extracellular varicosities or channels leading to blind ends. The Nernst–Planck equation with these geometrical factors incorporated is as follows:

$$J_K = -\frac{\alpha D}{\lambda^2}\left(c' + \frac{cV_o'}{\Psi}\right). \tag{17}$$

If there is no voltage gradient ($V_o' = 0$) this equation reduces to Fick's first law of diffusion, with the effective diffusion coefficient multiplied by a factor ($\alpha\lambda^{-2}$). The relation between Fick's first and second laws for diffusion of extracellular substances in brain tissue is discussed more fully by Gardner-Medwin (1980): in Fick's second law, D appears multiplied by a different factor (λ^{-2}). This distinction forms the basis for a method of measuring α and λ^2 in mammalian brain, yielding values *ca.* 0·2 and 2·5 respectively (Nicholson *et al.* 1979; Nicholson & Phillips, 1981).

In a situation with no gradient of $[K^+]_o$ (e.g. current passage under resting conditions) the K^+ flux is equal to the base-line K^+ transport number for the extracellular space (n_B) multiplied by I_o/F. This flux is also given under these conditions by eqn. (17), with $c' = 0$. Combining the two expressions, and using eqn. (4), we obtain a fixed relationship between the various parameters employed:

$$\frac{r_o \alpha D c_B F}{\lambda^2 \Psi} = n_B. \tag{18}$$

This relationship is used later to simplify other expressions.

Equations governing the rate of change of $[K^+]_o$

The K^+ concentration in a particular region of extracellular space is influenced by the following factors:

(i) *Release of K^+ into the extracellular space.* Potassium is added to the extracellular space at a rate Q moles per unit volume of tissue per sec, representing a disturbance of the tissue due to extrinsic K^+ sources (Lux & Neher, 1973) or neuronal activity. Processes of equilibration with cytoplasm will lead to temporary uptake of some of this K^+ into cells for as long as $[K^+]_o$ is elevated (ii), below). When release is due to neuronal activity there is in addition a component of uptake specifically in the active cells that is stimulated by Na_i gain and K_i loss, due partly at least to active transport (Cohen & de Weer, 1977). This 're-uptake' eventually restores all the lost K^+ to the active cells and will have the same spatial distribution as the initial release. The net effect on the rest of the tissue is as for an extrinsic K^+ load with Q positive and then negative with the same spatial distribution (pp. 417–419).

(ii) *Equilibration of extracellular K^+ with the cytoplasm of adjacent cells.* The assumption is made in many of the calculations (except where a non-zero value of τ_{eq} is stated) that changes of $[K^+]_o$ are accompanied by full equilibration of extracellular K^+ with a distribution space ξ times the tissue volume (p. 395). This means that there is an increase of tissue K^+ content (excluding the K^+ depletion that there may be in active neurones: (i) above) equal to $\xi\Delta c$. The differential equations for slow equilibration are dealt with on p. 405.

(iii) *Uptake or release of K^+ associated with membrane current in the transfer cells.* The rate of uptake from extracellular space per unit volume of tissue is given by ai_m/F, with i_m calculated from eqn. (16).

(iv) *Flux of K^+ between regions of extracellular space.* This is given by eqn. (17).

(v) *Changes of extracellular volume.* These changes are neglected (p. 397).

Bringing together the factors (i)–(v) above, we obtain an equation for the rate of change of the local K content of the tissue:

$$\xi\dot{c} = Q - \frac{ai_m}{F} - J_K'. \tag{19}$$

An expression for J_K' is obtained by differentiation of eqn. (17) and i_m is substituted from eqn. (16), giving:

$$\dot{c} = \frac{Q}{\xi} + \frac{\alpha D}{\xi\lambda^2}\left(c'' + \frac{cV_o''}{\Psi} + \frac{c'V_o'}{\Psi}\right) + \frac{a\Lambda^2 V_m''}{\xi F R_m}. \tag{20}$$

Using expressions for V_o' and V_o'' from eqns. (7) and (8) and simplifying the resultant with the definitions of Λ, T and β (p. 399) and eqn. (18), we obtain:

$$\dot{c} = \frac{Q}{\xi} + \frac{\Lambda^2}{T}\left[c'' + \frac{\beta V_m''(c_B - cn_B) - \beta c' n_B (V_m' + r_1 I)}{\Psi(1-n_B)}\right]. \tag{21}$$

This is the partial differential equation giving explicitly the rate of change of extracellular K^+ concentration for situations in which the distribution of extrinsic K^+ sources (Q) and of membrane potential of the transfer cells (V_m) are all known. As with the cable equation (eqn. (14)), it reduces to a linear approximation when the deviations from resting conditions are small:

$$\dot{c} = \frac{Q}{\xi} + \frac{\Lambda^2}{T}[c'' + \beta c_B V_m''/\Psi]. \tag{22}$$

Numerical solutions

Equations (14) and (21) (or their linearized equivalents, eqns. (15) and (22)) were solved simultaneously by Euler's method with the required initial and boundary conditions (see below). The intervals for spatial and temporal integration were in most cases $0{\cdot}2\Lambda$, $0{\cdot}01\tau$ and $0{\cdot}01T$ or $0{\cdot}1\Lambda$, $0{\cdot}002\tau$ and $0{\cdot}0005T$. Equation (14), governing the membrane potentials, was integrated to a steady-state solution between each of the steps used for eqn. (21), governing the changes of concentration. Relatively short time intervals ($\Delta t/\tau$, $\Delta t/T < (\Delta x/\Lambda)^2$) were required in eqn. (14) for convergence and in eqn. (21) for accuracy. Finite step size introduces errors that do not diminish with Euler's method unless integration is pursued to an intrinsically stable solution (as was the case for eqn. (14)). Checks were therefore made with critical results to see that halving the temporal and spatial intervals did not visibly alter the theoretical curves on scales appropriate for comparison with experimental data. Curves with $\beta = 0$ (simple diffusion: p. 405) were also compared with standard solutions. The curves are plotted through points centred on the spatial segments used in the calculations.

Some generality of the solutions was obtained by expressing the equations in terms of time in units of T and distance in units of Λ, and subsequently scaling the results. With the linear equations (15) and (22) the perturbations are all linear functions of the disturbing influence and scaling of the amplitude of the solutions was also possible. The generalized linear equations reduce to the following relatively simple form, with perturbations of V_m denoted by w (in units of Ψ: $w = (V_m - V_r)\Psi^{-1}$), the fractional increase of $[K^+]_o$ denoted by g ($= (c - c_B)c_B^{-1}$) and the K^+ source distribution denoted by q ($= QT(\xi c_B)^{-1}$ from eqn. (22)):

$$\tau\dot{w} = g - w + w'', \tag{23}$$

$$\dot{g} = g'' + \beta w'' + q(x,t). \tag{24}$$

There is only one tissue parameter (β) in these equations that affects the qualitative form of the solutions, apart from scaling, for any given source distribution or boundary condition. This parameter (β) is a measure of the flux carried by spatial buffer currents for long maintained gradients in the tissue, relative to that carried by extracellular diffusion. Only when $\beta = 0$ (no spatial buffering) do there appear to be any useful analytical solutions of these equations, when eqn. (24) reduces to the pure diffusion equation.

The linear equations (15) and (22) or their generalized forms (23) and (24) were employed for all the solutions used in this paper to compare the dynamics of K^+ with and without the effect of the transfer cells. The more complex non-linear equations (14) and (21), requiring substantially more computer time and specification of the amplitude of the disturbing influence and of V_r, were used for calculations involving comparisons with experimental data in the two preceding papers. In those papers the results for both the linear and non-linear calculations are illustrated, since this shows how the characteristics of the expected results arise chiefly from the simplest aspects of the model incorporated in the linear equations.

Boundary conditions

The equations are solved for various situations corresponding to (i) different distributions of K^+ sources and (ii) different boundary conditions. Source distributions (Q) are already incorporated in eqns. (21) and (22). The boundary conditions determine the calculation of $\dot{V}_m$ and $\dot{c}$ at both ends of the calculation domain, which extends from the brain surface (or K^+ source) to a depth (or radius) of at least ten space constants (Λ) of the transfer cells.

The boundary condition remote from the surface or the K^+ sources is set on the assumption that the tissue itself is many space constants thick. Under these conditions the effects of all the perturbations under consideration decline with distance (Δc, $\Delta V_m \rightarrow 0$ as $x \rightarrow \infty$) and are simply set to zero at the end of the calculation domain. When the calculated perturbations become significant within a few space constants of the far boundary (which sometimes occurred with prolonged perturbations) the calculations were repeated with the domain extended to 30 space constants.

The superficial segment of the calculation domain was subject to more complex boundary conditions. The equation for calculation of $\dot{V}_m$ (eqn. (14) or (15)) was modified to take account of the fact that the transfer cells terminate at this point in closed ends and the consequent constraint that the extracellular current is here equal to the total current (I) across the tissue surface. Direct accounting for all the currents in the superficial segment with the conventional methods of cable analysis leads to alteration of the term $\Lambda^2 V_m''$ in eqn. (6), and consequently in eqns. (14) and (15) to $\Lambda^2(V_m' - r_o I)\,\Delta x^{-1}$, where Δx is the width of the superficial segment (normally $0{\cdot}2\Lambda$).

In the calculation of c at the surface it was assumed that $[K^+]_o$ in the superficial segment was identical to that in a well stirred superfusion fluid with either constant or deliberately altered composition. Calculations with conditions corresponding to a diffusion barrier at the surface were made but are not presented in this paper since they did not give a better fit to any of the data than was obtained without a diffusion barrier.

For comparison with results obtained by Gardner-Medwin (1983) it was necessary to calculate the net flux exchanged between the tissue and surface fluid. The value of c in the superficial segment, determined by the boundary condition, was compared at each step with the value it would have taken if there had been no surface flux since the previous step (eqn. (25), below). The difference multiplied by $\xi\Delta x/\Delta t$ gave the flux per unit area of tissue.

Symmetrical source distributions were treated by imposing a condition that there be zero flux at the origin, corresponding to the centre of symmetry. The modified version of eqn. (21) for the first segment under these conditions is:

$$\dot{c} = \frac{Q}{\xi} + \frac{\Lambda^2}{T\Delta x}\left[c' + \frac{\beta(c_B - cn_B)(V_m' - Ir_o)}{\Psi(1-n_B)} - \frac{cIr_o}{\Psi}\right]. \tag{25}$$

Modifications for radial solutions

The one-dimensional analysis in the foregoing sections can be repeated with only slight modifications for situations with radial symmetry, in which the variables in the tissue are the same at all points equidistant from a centre of symmetry and in which the total current radiating from the centre (and not the current density) is the same at all distances. The results of this modified analysis are stated here without derivation.

If I_R is the total radial current and x is the distance measured from the centre, V_m'' in eqns. (14), (15), (21) and (22) is replaced by $(V_m'' + 2x^{-1}V_m')$, c'' in eqns. (21) and (22) replaced by $(c'' + 2x^{-1}c')$ and I in eqn. (21) replaced by $I_R\,(4\pi x^2)^{-1}$.

The boundary conditions for radial solutions are also modified in a similar manner to take account of the special conditions at the centre of symmetry. The term $\Lambda^2 V_m''$ in eqns. (14) and (15) becomes, for the central segment, $\Lambda^2(3V_m'/\Delta x - 3r_o I_R/(4\pi\Delta x^3))$. There is no realistic situation corresponding to a condition with fixed $[K^+]_o$ at the central point: either there is zero flux entering the central point or a flux determined by the characteristics of a point source, such as an ionophoretic electrode or a small region of active tissue. Equation (25) was modified to calculate the changes of c in the central segment when there was zero flux by substitution of $\Delta x/3$ for Δx and $(I_R/4\pi\,(\Delta x)^2)$ for I. Any flux at the central point is treated as a K^+ source within the central segment.

Modifications for slow equilibration of extracellular space and cytoplasm

Equations (19)–(25) were derived with the assumption that a change in $[K^+]_o$, Δc, is associated at all times with a change $\xi\Delta c$ in the local K^+ content of the tissue. Part of the distribution space represents cytoplasmic K^+ that may be expected to equilibrate at a finite rate with changes of $[K^+]_o$.

Several processes contribute to K^+ uptake (Gardner-Medwin, 1980). It is assumed here that, once a steady state is established, the increase of cell K^+ content is proportional to Δc and that the equilibration is governed by a single exponential time constant τ_{eq}. These are likely to be approximations because of non-linearities in the dependence of Na–K pump rates and membrane currents on extra- and intracellular K^+ concentrations.

For slow equilibration we can replace the tissue distribution space for K^+ (ξ) in eqn. (19) by the extracellular component (α), adding at the same time a term for the rate of K^+ uptake into the cytoplasm (Z) per unit volume of tissue:

$$\alpha\dot{c} = Q - ai_m/F - J_K' - Z. \tag{26}$$

The cytoplasmic distribution space is $(\xi-\alpha)$, so if s is the effective concentration within that space the uptake is given by:

$$Z = (\xi-\alpha)\,\dot{s}. \tag{27}$$

The assumption of exponential equilibration is represented by the equation:

$$\dot{s} = (c-s)/\tau_{eq}. \tag{28}$$

Substitution of eqn. (27) in eqn. (26) gives:

$$\dot{c} = \alpha^{-1}(Q - ai_m/F - J_K' - (\xi-\alpha)\,\dot{s}). \tag{29}$$

Equation (28) was solved simultaneously with eqn. (29), using the standard substitutions already used to derive eqns. (21), (22) and (25) from eqn. (19).

Meaning of the compound parameters Λ, T and β

In the equations governing K^+ dynamics in the model, the tissue parameters appear principally in combinations defined as Λ, T and β (p. 399). These are the principal parameters that must be assigned values for a comparison of calculated solutions with experimental data and it is therefore important to consider their physical meaning.

Λ is a parameter that arises naturally in the cable analysis for the transfer cells (p. 400). It is the space constant for the electrotonic decline with distance, through undisturbed tissue in the steady state, of any small disturbance of the membrane potential (V_m) of the transfer cells. This can be seen most simply from eqn. (15) putting $\tau\dot{V}_m = 0$ and $c = c_B$. Note that this space constant depends not only on the properties of the transfer cells, but also on the extracellular resistance (r_o). If there were a diminution of extracellular space fraction (α), r_o would increase and Λ would decrease.

T is a characteristic time for the tissue that depends on the extent of cytoplasmic equilibration (ξ) and on the extracellular diffusion parameters (D, α, λ: p. 402). Its chief role is in equations giving the rate of change of $[K^+]_o$, particularly eqn. (21). If we omit from this equation the terms associated with K^+ sources and with spatial buffering by the transfer cells (putting $Q = \beta = 0$), we obtain the conventional diffusion equation with an effective diffusion constant equal to $(\Lambda^2 T^{-1})$. Thus, referring to Carslaw & Jaeger (1959: section 2·4), we can say that T is the time it would take for the K^+ concentration at a depth Λ beneath the tissue surface to become approximately 52% equilibrated with an altered concentration at the surface *if* K^+ flux were solely by extracellular diffusion. In practice equilibration will be somewhat faster than this if spatial buffering makes a significant contribution to the K^+ transfer into the tissue (p. 409).

β is a dimensionless parameter that is a measure of the relative importance of the transfer of K^+ through the transfer cells compared to extracellular diffusion. If $\beta = 0$ there is no spatial buffering (see below) and all the equations for K^+ changes reduce to simple diffusion equations. If we describe the K^+ flux through the tissue expected by extracellular diffusion alone as the *expected flux* and the difference between this and the actual flux as the *extra flux*, then β is in some simple situations the quotient: *extra flux/expected flux*. This means that the factor by which the actual flux is greater than the expected flux is $(\beta+1)$. The situations for which this is the case are described on pp. 408, 419: in general they are ones in which the gradients of driving force for K^+ flux (either

a potential gradient or a concentration gradient in the extracellular space) are maintained through the tissue over distances of several space constants (Λ) of the transfer cells.

Solutions of the equations above are presented in the Figures below in terms of units involving Λ and T. Results calculated with and without transfer of K^+ by the spatial buffer mechanism must be compared on the same absolute scales. To achieve this, β is set to zero with no change of Λ or T. From the definition on p. 399, $\beta = (n_B^{-1} - 1)\, r_o/(r_i + r_o)$. Since r_o cannot be zero, $\beta = 0$ implies that $r_i = \infty$. There is therefore no current in the transfer cells (eqn. (3)) and no spatial buffer action. Equation (19), governing the changes of $[K^+]_o$, retains only the K^+ source and diffusion terms. The diffusion term ($\Lambda^2 c''/T$) incorporates the transfer cell space constant Λ; but from the definition of T on p. 399, Λ^2/T is equal to the appropriate diffusion coefficient $\alpha D \lambda^{-2} \xi^{-1}$. The parameters Λ and T are used to normalize the equations (p. 403), so when $\beta = 0$ it is convenient to retain them with the same values to obviate rescaling, despite the fact that in this situation the transfer cells have no effect on $[K^+]_o$. Physically, the situation in which $\beta \to 0$ while Λ is constant corresponds to reducing the number of transfer cells to zero, while keeping their space constant unchanged. The total cross-sectional area and membrane area (a) of the transfer cells tend to zero. Since the internal resistance of the transfer cells (r_i) varies inversely with their area (p. 400), $r_i \to \infty$ and Λ, T remain constant if R_m is adjusted slightly to keep $R_m a^{-1}(r_i + r_o)^{-1}$ constant (p. 399). Other limiting cases with no spatial buffering (e.g. R_m, $\Lambda \to \infty$) would give similar results but would require rescaling of the Figures presented for changes in Λ, T.

RESULTS

The effects of current flow through the tissue

It is possible to envisage fairly simply in qualitative terms what happens when a current is passed through a region of tissue and out across its surface. Close to the surface the current is carried entirely in extracellular space, while deeper within the tissue it flows partly through the cytoplasm of the syncytium of transfer cells (Fig. 1*D*). Within a few space constants (Λ) of the surface, the current leaves the transfer cells across their membranes. When the current is first turned on, this membrane current and the associated disturbance of membrane potential (depolarization, in the case of current flowing out across the tissue surface) fall off exponentially with depth from the surface. This pattern of currents is shown diagrammatically in Fig. 1*D*, with the calculated change of membrane potential plotted in Fig. 2*A* (continuous line: $t = 0$). The current which leaves the syncytium of cells near the surface must enter them elsewhere. The boundary conditions for the calculations employed here (p. 404) amount to assuming that the tissue surface at which the current enters is sufficiently remote (several space constants, Λ, away) that the consequences at the two surfaces can be examined independently.

Since the total extracellular current at the tissue surface is greater than it is deep within the tissue (Fig. 1*D*), the gradient of extracellular voltage is not precisely uniform. In order to account for the data from the rat brain (Gardner-Medwin, 1983) only about 6% of the current need be assumed to flow within the transfer cells deep in the tissue and the slight discrepancy of the graph of the extracellular voltage (V_o) against depth (Fig. 2*B*, continuous line) from the straight line expected with no current through transfer cells (dashed line, Fig. 2*B*) is too small to be straightforwardly detectable. The significance of this small current flowing through transfer cells is indicated, however, by the other types of data and effects to be described.

If the pattern of currents shown in Fig. 1*D* is maintained for some time, the K^+ efflux carried by the current across the transfer cells causes a cumulative build-up of K^+ in the extracellular space near the surface. The distribution of this build-up

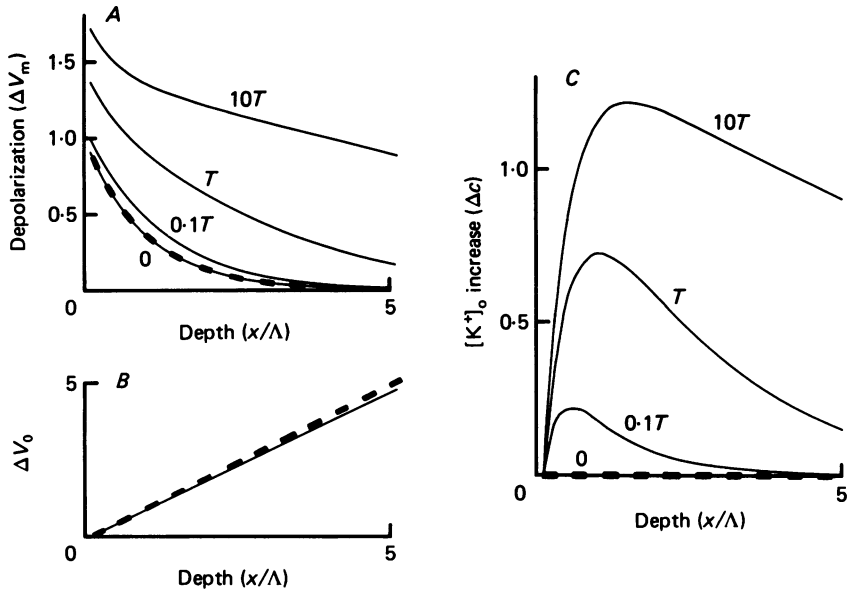

Fig. 2. Effects of current passage outward across the tissue surface, plotted against depth (x) from the surface. Dashed lines: with no K^+ flux through the transfer cells ($\beta = 0$); continuous lines: $\beta = 5$. *A*, depolarization of the transfer cells at stated times after current onset (units: $\Lambda r_0 I$). Dashed line applies for all $t > 0$. *B*, extracellular potential relative to the tissue surface (units: $\Lambda r_0 I$). Note that the curves for $t = 0$ to $t = 10T$, if superimposed, would not be resolvably different. *C*, extracellular K^+ concentration changes at stated times (units: $c_B \Lambda r_0 I \Psi^{-1}$). Note that there are no concentration changes for $\beta = 0$. Calculations with linearized equations; depth intervals 0·2 Λ; lower boundary condition at 30 Λ.

is initially an exponential function of depth, just as is the distribution of current that causes it. The K^+ does not simply go on accumulating where it enters the extracellular space, however: it diffuses to regions where there is less concentration change, towards the tissue surface (where it is assumed to be sufficiently rapidly diluted in fluid at the surface that the concentration change is zero) and towards deeper regions of the tissue. The consequent profiles of the $[K^+]_o$ increase, plotted against depth, are shown for various times after the onset of current in Fig. 2*C* (continuous lines). As time progresses, the concentration change becomes greater, and also more spread out in depth. This progressive change in K^+ concentration profile is reflected also in the distribution of membrane potential of the transfer cells (Fig. 2*A*) which become depolarized as a result of the raised extracellular K^+ concentration as well as the current flow.

The continuous lines in Figs. 2–4 are calculated with the linear equations with $\beta = 5$, which fits approximately the data of Gardner-Medwin (1983) for rat brain. The dashed lines show calculations plotted on the same scales for $\beta = 0$, i.e. with extracellular diffusion alone (p. 405). Comparison of the two sets of curves shows the effects of current-mediated K^+ flux through the transfer cells. Note that even when $\beta = 0$ it is possible to plot the depolarization of the transfer cells (Fig. 2*A*, dashed line), though these cells can only exist either with extreme properties or in insignificant numbers (p. 406).

K^+ flux within the tissue during current flow is due partly to the current and voltage gradients themselves and partly to the extracellular concentration gradients, which we have seen develop gradually and primarily close to the surface (Fig. 2*C*). Deep within the tissue the concentration gradients are negligible. The fraction of the total tissue current that passes through cytoplasm in the deep tissue is given by the

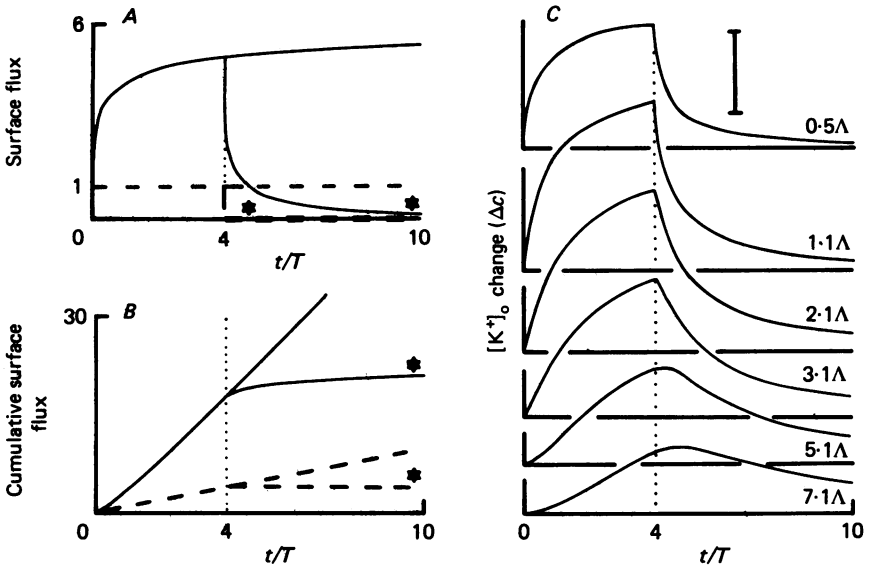

Fig. 3. Flux and concentration changes produced by current flow, plotted as functions of time after current onset. *A*, outward surface K^+ flux produced by current outward across the surface. Curves are plotted for current maintained to $t = 10T$ and for current switched off at $t = 4T$. Continuous lines: $\beta = 5$; Dashed lines: $\beta = 0$; units: $n_B IF^{-1}$. *B*, total K^+ passed across the tissue surface since current onset (i.e. integrals of curves in *A*). Units: $n_B ITF^{-1}$. *C*, extracellular K^+ concentration changes produced at stated depths for current passed from $t = 0$ to $t = 4T$; vertical calibration: $0{\cdot}5\, c_B \Lambda r_o I/\Psi$; $\beta = 5$. Calculations as for Fig. 2.

resistance ratio $r_o/(r_i + r_o)$ and in the model represents entirely K^+ transfer (p. 397). The extracellular current (a fraction $r_i/(r_i + r_o)$ of the whole) is only partly due to K^+ flux (a fraction n_B: the K^+ transport number in extracellular fluid). Thus the total K^+ transfer deep within the tissue is equivalent to a fraction $(n_B r_i + r_o)/(r_i + r_o)$ of the total tissue current. From the definition of β (p. 399) this can be shown by simple algebraic manipulation to be equal to $(\beta + 1)n_B$, or $(\beta + 1)$ times the expected fraction of the current that would be accounted for by K^+ flux if only extracellular space were involved. This shows that measurement of the flux of K^+ through the tissue could be a straightforward way of measuring β. It is not possible for technical reasons, however, to measure the K^+ flux deep within the tissue directly. The flux across the *surface* can be measured (Gardner-Medwin, 1983) and with the numerical model the expected surface flux can be calculated (Fig. 3*A*). Some of the K^+ that is transferred by cytoplasmic current from deep down in the tissue to be released into the extracellular space near the surface (Fig. 1*D*) diffuses backwards, however, and does not cross the tissue surface. This explains why the initial surface K^+ flux is less than

($\beta+1$) times the flux for extracellular transport alone and only approaches this value asymptotically if the current is maintained (Fig. 3*A*).

Fig. 3*B* shows the cumulative flux across the surface in these calculations, analogous to the results obtained with collection of K^+ in a well stirred surface cup (Gardner-Medwin, 1983). In each case, graphs are shown for currents terminated at an arbitrary time ($4T$ after onset) as well as for maintained currents. This shows how some efflux from the brain persists after the end of the current period, while the K^+ that has built up within the tissue continues to diffuse across the surface and into the deeper tissue. Fig. 3*C* shows the build-up and decline of $[K^+]_o$ with such a protocol, calculated at various depths within the tissue. These graphs are analogous to the observations made with K^+ sensitive micro-electrodes by Gardner-Medwin & Nicholson (1983) and show a number of qualitative features present in the experimental records. The initial rate of rise of the K^+ concentration is highest near the surface, but in this region shows marked saturation as the current is maintained. Deeper in the tissue, the slower initial rates of rise are maintained for longer. At the deepest levels the K^+ concentration even continues to rise for a period after the termination of the current. The depth dependence of the initial rate of rise of the K^+ concentration changes allows an estimate of the space constant (Λ) of the transfer cells to be made, which in the rat cerebellum is *ca.* 0·2 mm (Gardner-Medwin & Nicholson, 1983).

Effects of superfusion of the surface with altered K^+ concentration

Superfusion is a simple way of altering $[K^+]_o$ in the tissue. Transfer of K^+ to or from the extracellular space occurs both by diffusion and by operation of the spatial buffer mechanism through the transfer cells (Fig. 1*C*). The resulting profiles of $[K^+]_o$ as a function of depth are plotted in Fig. 4*A* for various times after the onset of a change, with $\beta = 5$ (continuous lines) and with $\beta = 0$ (dashed lines). The results for $\beta = 0$ are simply solutions of the diffusion equations, for diffusion in extracellular space with reversible uptake into cytoplasm, and are of the form given in Carslaw & Jaeger (1959, p. 60):

$$\Delta c = \Delta c_0 \operatorname{erfc}\left[\frac{x/\Lambda}{2(t/T)^{\frac{1}{2}}}\right]. \tag{30}$$

With spatial buffering (continuous lines, Fig. 4*A*) the changes of $[K^+]_o$ deep in the tissue occur faster because the flux to these regions is greater. Near the surface the K^+ concentration is less than with pure diffusion. This is because K^+ transport into these regions occurs only across the surface by diffusion while the flux away from them to deeper tissue is augmented by the spatial buffer mechanism (Fig. 1*C*). The flux across the surface (Fig. 4*B*) is proportional to the gradient of K^+ concentration near the surface, and is greater with spatial buffering than without.

The currents associated with the spatial buffer process generate voltage gradients in the extracellular space (Fig. 1*C*). The extracellular voltage relative to deep tissue is shown as a function of time in Fig. 4*C*, for various depths (continuous lines, with $\beta = 5$). If the spatial buffer mechanism makes no contribution to flux ($\beta = 0$), then only small diffusion potentials occur, as a result of the unequal aqueous mobilities of the ions with extracellular concentration gradients. The hatched area in Fig. 4*C* shows the range of diffusion potentials between the surface and deep tissue if the

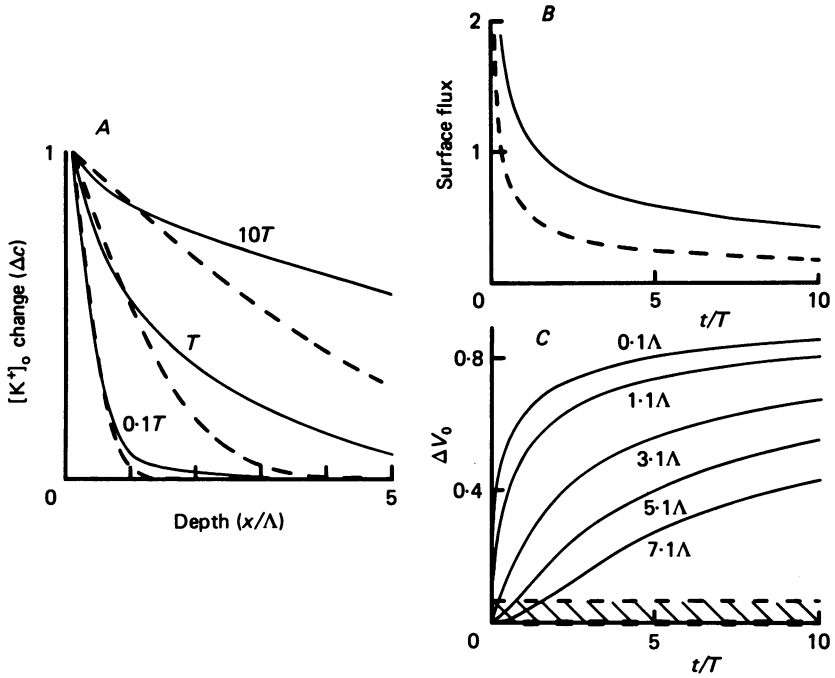

Fig. 4. Changes following alteration of K^+ concentration at the tissue surface. Continuous lines: $\beta = 5$; dashed lines: $\beta = 0$. *A*, concentration changes as a function of depth at various stated times. Units: fraction of surface change (Δc_0). *B*, inward flux across the tissue surface as a function of time. Units: $\alpha D\lambda^{-2}\Lambda^{-1}\Delta c_0$. *C*, extracellular potential change relative to deep tissue for tissue segments centred at the stated depths (x). Units: $\beta n_B \Psi(1-n_B)^{-1}\Delta c_0/c_B$. Hatched area gives the range of surface potential changes expected for diffusion potentials alone ($\beta = 0$). Calculations as for Fig. 2.

alterations of K^+ concentration are by K/Na substitution alone (upper limit) or by changes of KCl concentration (lower limit). These are calculated from the Planck–Henderson equation (Bockris & Reddy, 1970, p. 481) and they represent the full potential difference between the surface and deep tissue, comparable with the potentials calculated with spatial buffering for the superficial segment ($0{\cdot}1\Lambda$). Measurements of the time course of the surface potential change have been made in various tissues (Gardner-Medwin, Gibson & Willshaw, 1979; Gardner-Medwin, 1983). It develops gradually, as in Fig. 4*C*. The final level gives a measure of β since with small concentration changes ($\Delta c/c \ll 1$) it is equal to $\beta n_B(1-n_B)^{-1}\Psi\Delta c/c$. The time course of the voltage change depends on T, with approximately 64% of the final change occurring at $t = T$. The gradual development of the voltage gradient is due to the fact that the spatial buffer mechanism cannot act straight away when there is a change in concentration at the surface. Initially K^+ can only diffuse into the superficial tissue. It is only when $[K^+]_o$ is raised over a depth range of more than one space constant (Λ) that the superficial depolarization of the transfer cells approaches its full value and provides the full driving force for the spatial buffer mechanism and for the extracellular voltage gradients.

These results (Figs. 2–4) are all calculated on the assumption that there is no

significant barrier to diffusion of K^+ localized at the tissue surface. Fisher *et al.* (1976) interpreted the results in superfusion experiments to indicate that there is such a barrier. Their data were obtained with ion-selective micro-electrodes at various depths beneath the surface of the cat cortex after superfusion with saline containing 12 mM-K^+. Fig. 5 (large circles) shows the average data (from their Fig. 7*a*) reproduced as a function of depth beneath the cortex, for measurements made at an

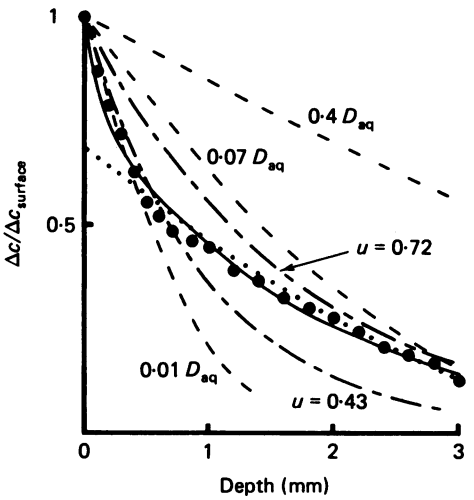

Fig. 5. Extracellular concentration changes as a function of depth during superfusion with altered $[K^+]$. Circles: data from Fisher *et al.* (1976), Fig. 5, at an average time 3·7 hr after the start of superfusion with $[K^+] = 12$ mM: neocortex of cat anaesthetized with pentobarbitone; cup diameter 7 mm; replotted as $(c-c_B)\ c_B^{-1}$ where c_B is taken as the observed average base line $[K^+]_o$ (3·15 mM). Equal dashes: Erfc curves expected at 3·7 hr for simple diffusion with effective diffusion coefficients (i.e. $\alpha\xi^{-1}\lambda^{-2}\ D$) equal to 0·4, 0·07, 0·01 times D_{aq}. The upper curve is that expected for an extracellular marker ($\alpha = \xi$; $\lambda^{-2} = 0{\cdot}4$). Dots: curve expected with diffusion ($\alpha\xi^{-1}\lambda^{-2}D = 0{\cdot}11\ D_{aq}$) with a surface barrier ($h = 0{\cdot}8\ mm^{-1}$), as fitted by Fisher *et al.* (1976). Unequal dashes: exponential curves expected in a steady state if K^+ transfer occurs by extracellular diffusion ($\alpha = 0{\cdot}2$; $\lambda^2 = 2{\cdot}5$) and there is loss of K^+ to the blood at a rate u. Δc where $u = 0{\cdot}72$, $0{\cdot}43\ hr^{-1}$. Continuous line: steady state calculated with $u = 1{\cdot}3\ hr^{-1}$ and with flux through the tissue occurring by spatial buffer transfer ($\beta = 5$, $\Lambda = 0{\cdot}2$ mm) as well as extracellular diffusion.

average time of 3·7 h after the change of surface concentration. Fisher *et al.* pointed out that the data cannot be fitted with erfc solutions for simple diffusion with any choice of diffusion coefficient (single dashed lines, Fig. 5). Four factors might contribute to this discrepancy from simple diffusion: (i) equilibration of extracellular K^+ with cytoplasm, (ii) a surface diffusion barrier, (iii) clearance of K^+ into the blood and (iv) transfer of K^+ by the spatial buffer mechanism. Cytoplasmic equilibration (pp. 395, 421–422) increases the distribution volume for K^+ in the tissue and lowers the effective diffusion coefficient, but does not alter the form of the expected concentration profiles. Diffusion combined with a postulated surface barrier can improve the fit of the data in deep tissue though not over the whole range (dotted line, using parameters for the best fit of this kind proposed by Fisher *et al.* (1976)). Clearance from tissue into blood would lead eventually to a steady concentration profile, associated with

a balance between clearance and flux into the tissue (Fenstermacher, Patlak & Blasberg, 1974). Fig. 7*b* of Fisher *et al.* (1976) suggests that at least at some depths a practically steady concentration would have been reached at the time (3·7 hr superfusion) when the concentration profile was obtained. Fig. 5 compares the data with a steady-state profile (continuous line) calculated by assuming that clearance occurs at a rate proportional to the excess of $[K^+]_0$ over its base-line value ($Q = -u.\Delta c$) and that K^+ flux occurs by both diffusion and the spatial buffer mechanism, with the parameters derived for rat brain ($\beta = 5$; $\Lambda = 0{\cdot}2$ mm). A reasonable fit is obtained with $u = 1{\cdot}3$ hr^{-1} (Fig. 5), which would imply a K^+ clearance into the blood of 4·0 m-mole hr^{-1} per kg tissue per 3 mM change of $[K^+]_0$. This is a plausible figure since it is of the same order of magnitude as the normal exchange of K^+ across the blood–brain barrier (2·9–3·6 m-mole kg^{-1} hr^{-1}) measured with radioactive techniques under base-line conditions ($[K^+]_0$ *ca.* 3 mM) in the rat (Katzman & Leiderman, 1953). Inclusion of the spatial buffer contribution to K^+ flux is an essential element in obtaining the satisfactory fit shown by the full line in Fig. 5, since a steady state with clearance and diffusion alone (yielding the equation $Dc'' = u\Delta c$) would theoretically correspond to one of a family of exponential profiles (double-dashed lines, Fig. 5) that fail to show the marked increase in the gradient of $[K^+]_0$ exhibited by the data close to the surface. The model represented by the continuous line in Fig. 5 is not the only one that might fit these data: see Gardner-Medwin (1981*b*) for an alternative involving an extreme choice of intrinsic tissue parameters without clearance of K^+ into the blood. The fact that a fit can be obtained with established mechanisms and plausible parameters suggests that there is no reason to invoke a surface barrier in attempting to explain these data.

Ionophoretic point source release of potassium

Following Lux & Neher (1973) there have been several studies of extracellular space using ionophoretic release of marker ions and detection of their concentration build-up a short distance away (Nicholson *et al.* 1979; Dietzel *et al.* 1980; Nicholson & Phillips, 1981). The behaviour of potassium has been found to be anomalous (Nicholson *et al.* 1979), suggesting that it does not remain even for short times principally in extracellular space. This anomaly was overlooked by Lux & Neher (1973) because they were not using truly extracellular ions for comparison with K^+. The data of Lux & Neher (1973) is re-examined here in relation to the present model for K^+ dynamics.

Fig. 6 shows data replotted from Fig. 2*a* of Lux & Neher (1973). Measurements of K^+ concentration rises were made approximately 40 μm from a micro-electrode tip through which a current was passed to release K^+, both in saline (open circles) and in the cat neocortex (filled circles). Different current strengths (320 nA, 80 nA) were used in saline and in the tissue: the concentration increases are plotted here per 100 nA of current. A complementary error function curve (dotted line) was fitted to the measurements in saline and the corresponding curves (dashed lines) are calculated for the results expected in the brain tissue on various hypotheses. The upper curve is a complementary error function with time course 2·5 times longer and amplitude 12·5 times greater than the saline results; this is the curve expected for an extracellular marker in the tissue with $\alpha = 0{\cdot}2$, $\lambda^2 = 2{\cdot}5$, agreeing with the data obtained in similar experiments with tetraethyl- and tetramethylammonium ions

(Nicholson *et al.* 1979; Nicholson & Phillips, 1981). The lowest curve is calculated with the assumption that these extracellular parameters still apply, but that in addition there is K^+ transfer by the spatial buffer mechanism ($\Lambda = 0{\cdot}1$ mm, $\beta = 5$) and reversible cellular uptake ($\xi = 1$, $\tau_{eq} = 7$ sec: p. 405). This combination provides a

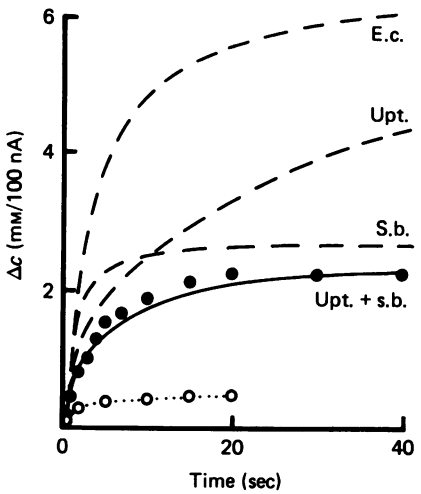

Fig. 6. $[K^+]_o$ changes near an ionophoretic point source of K^+. Circles: data from Lux & Neher (1973, Fig. 2*a*) showing measurements in the neocortex of a cat anaesthetized with pentobarbitone (●) and in saline (○), replotted as $[K^+]_o$ increases per 100 nA ionophoretic current; actual currents: 80 nA (tissue) and 320 nA (saline); nominal electrode separation 40 μm. Dotted line: diffusion solution (erfc) fitting the saline data, derived for $D = 1{\cdot}85$ cm^2 sec^{-1} (see Lux & Neher (1973): as for saline at 20 °C); $r = 50$ μm; transport number for ionophoretic K^+ release = 0·6. Other curves are $[K^+]_o$ changes expected in brain tissue with various assumptions in the present model. E.c.: assuming dispersal by extracellular diffusion alone, with $\alpha = 0{\cdot}2$, $\lambda^2 = 2{\cdot}5$ (Nicholson *et al.* 1979). Upt.: dispersal by extracellular diffusion with reversible K^+ uptake ($\xi = 1{\cdot}0$; $\tau_{eq} = 7$ sec). S.b.: dispersal by extracellular diffusion and spatial buffer transfer ($\beta = 5$; $\Lambda = 0{\cdot}1$ mm) with no cellular uptake. Upt. + s.b.: with the preceding mechanisms combined. Linear calculations; 0·1 Λ radial steps; boundary conditions at 15 Λ radius.

reasonable fit to the data. The other curves show that neither the inclusion of the spatial buffer mechanism alone nor of reversible uptake alone can account for the data. The first lowers the expected final amplitude of the concentration changes as required, but fails to reduce them earlier, before K^+ has diffused far enough for the spatial buffer mechanism to become effective (cf. p. 410). The uptake hypothesis on its own reduces the initial but not the final amplitude. Additional complications may arise from disturbances of K^+ dynamics due to cellular damage in the small but critical region around the electrodes. The space constant for the spatial buffer mechanism required to fit the data ($\Lambda = 0{\cdot}1$ mm) is smaller than that derived from other observations (Gardner-Medwin & Nicholson, 1983: $\Lambda = 0{\cdot}2$ mm). Thus the full range of factors that may be involved in accounting for these experimental results would require further study for its elucidation; but those considered in the present model are at least qualitatively of the type that would account for the different behaviour of K^+ and extracellular markers.

Distributed, steady K^+ sources

Release of K^+ into extracellular space throughout an extensive region may occur during neuronal activity and in pathological situations associated, for example, with spreading depression, ischaemia and trauma. The circumstances in which dispersal and uptake mechanisms play significant roles in affecting $[K^+]_o$ with such distributed sources are identified here. Only simple geometrical situations are treated: spherical zones of release in the midst of a large (effectively infinite) volume of tissue with uniform properties. In this section continuous steady sources starting at time zero are considered; in the following section (p. 415) brief periods of release and release followed by re-uptake are considered.

The changes of $[K^+]_o$ are calculated, for comparison, with up to four different sets of assumptions. These represent (i) the behaviour expected for an ion remaining in extracellular space ($\beta = 0$; $\xi/\alpha = 1$; $\alpha = 0{\cdot}2$; $\lambda^2 = 2{\cdot}5$), (ii) extracellular diffusion augmented by the spatial buffer mechanism ($\beta = 5$; $\Lambda = 0{\cdot}2$ mm), (iii) extracellular diffusion combined with reversible cytoplasmic uptake ($\xi = 1$; $\tau_{eq} = 22$ sec) and (iv) with all mechanisms combined. In the Figures the curves for these various assumptions are labelled respectively e.c., s.b., upt. and s.b. + upt. The parameters for extracellular space are from Nicholson & Phillips (1981); those for the spatial buffer mechanism and for ξ are those that fit the data in the accompanying papers (see Discussion). The time constant for cytoplasmic equilibration (τ_{eq}) has been set to roughly the correct order of magnitude (p. 422), which is small enough that smaller or moderately larger values would make practically no difference to the results presented in the present section.

Fig. 7 shows results calculated for a steadily maintained source of diameter 0·8 mm. The graphs show the concentration rise (Δc) at the centre as a function of time after the start of release, in units of mM for a total release of 1 p-mole sec^{-1}. Comparing the upper curve (extracellular diffusion alone) with the continuous line (s.b. + upt.), a reduction of Δc by a factor of about 4 due to the combined buffering action is evident at all times from a few seconds to 1000 sec. The curves for the two buffering mechanisms separately show that the overall reduction is due principally to spatial buffer action for times greater than 75 sec and principally to uptake for the shorter times. At $t = 75$ sec the reduction achieved by each mechanism on its own is 61 % and in combination 76 %.

The percentage reduction of Δc achieved through buffering action at the centre of a release zone is much diminished if the zone is small. With a diameter of 0·08 mm instead of 0·8 mm the reduction at 75 sec is only 19 % due to s.b. action, 8 % due to uptake and 21 % with both mechanisms in combination. In this situation the central rise is largely determined by the characteristics of diffusion. Nevertheless, the buffering mechanisms act to restrict the volume of tissue outside the release zone that is affected by the disturbance. Fig. 8 shows the volume of tissue affected by different levels of concentration rise with and without buffering action, for a range of times after the onset of release and for two different source diameters (0·8 and 0·08 mm). For clarity, only results for the combined buffering action are illustrated. The reductions at the shortest illustrated time (22 sec) are due principally to uptake and at the two longer times to spatial buffering. At the centre of the 0·08 mm diameter

release zone (circles: Fig. 8*B*) the calculated rise of $[K^+]_o$ without buffering is 16–18 mM, while with buffering it is 13–15 mM (after release at 1 p-mole sec for 22–2200 sec). The volume of tissue affected by a rise of 1 mM or more is reduced substantially, however: by 91% at 220 sec (from 0·094 mm^3 to 0·0084 mm^3). The reduction of the number of cells affected by a localized source may be an important beneficial consequence of buffering.

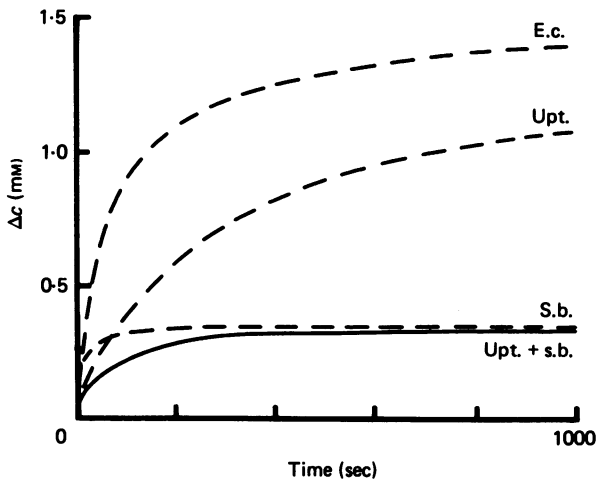

Fig. 7. $[K^+]_o$ changes with a distributed source. Δc is calculated with various assumptions, for the centre of a spherical region 0·8 mm in diameter in which there is a steady uniform release of K^+ starting at time zero. E.c.: K^+ dispersal by extracellular diffusion ($\alpha = 0{\cdot}2$, $\lambda^{-2} = 0{\cdot}4$), with no cellular K^+ uptake. Upt.: assuming cytoplasmic K^+ uptake ($\xi/\alpha = 5$; $\tau_{eq} = 22$ sec), with dispersal by extracellular diffusion alone. S.b.: assuming no uptake, but dispersal by extracellular diffusion and spatial buffering ($\beta = 5$, $\Lambda = 0{\cdot}2$ mm, $T = 220$ sec). Upt. + s.b.: with the preceding mechanisms combined. Linear calculations; 0·2 Λ radial steps; boundary conditions at 30 Λ radius. Units: mM for a total release rate of 1 p-mole sec^{-1} ($Q = 3{\cdot}7$ μmole $l.^{-1}$ sec^{-1}).

There is always a region of distant tissue in which the spatial buffer mechanism acts to increase rather than to decrease Δc, where the K^+ dispersed by spatial buffer action is released into extracellular space. This occurs beyond the range of the results shown in Fig. 8 and is generally in tissue where the increase of $[K^+]_o$ is itself relatively small.

Decline of $[K^+]_o$ after release

The decline of $[K^+]_o$ after the end of a period of K^+ release is influenced by all the factors that affect K^+ build-up during release. In addition it may be hastened significantly by re-uptake of K^+ into neurones from which the release occurred, leading sometimes to an undershoot of $[K^+]_o$ below base line. Decline is first considered here without re-uptake.

Fig. 9*A* shows Δc after an instantaneous release of K^+ into extracellular space throughout a spherical zone with diameter 0·8 mm. Δc at the centre of the zone is plotted as a fraction of its initial value, with parameters as in the last section. If the

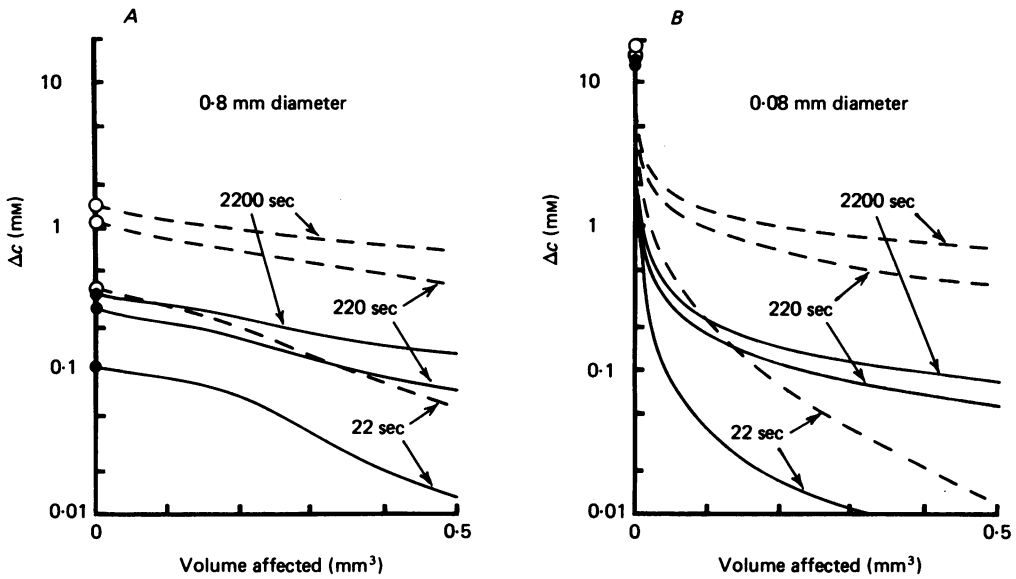

Fig. 8. Effect of buffering on the amount of tissue affected by concentration rises when there is a maintained K^+ source. Δc at radii up to 0·5 mm from the centre of a source with diameter *A*, 0·8 mm and *B*, 0·08 mm is plotted against the volume of tissue enclosed by a sphere at each radius (i.e. the volume affected by equal or larger concentrations rises). Plots are given for three indicated times after the start of release and for two conditions: dashed lines and ○, extracellular dispersal only; continuous lines and ●, spatial buffer and cytoplasmic uptake mechanisms together, with parameters as for Fig. 7. Units: mM for a total release rate of 1 p-mole sec^{-1}. (Note, ○ and ● are on the axis).

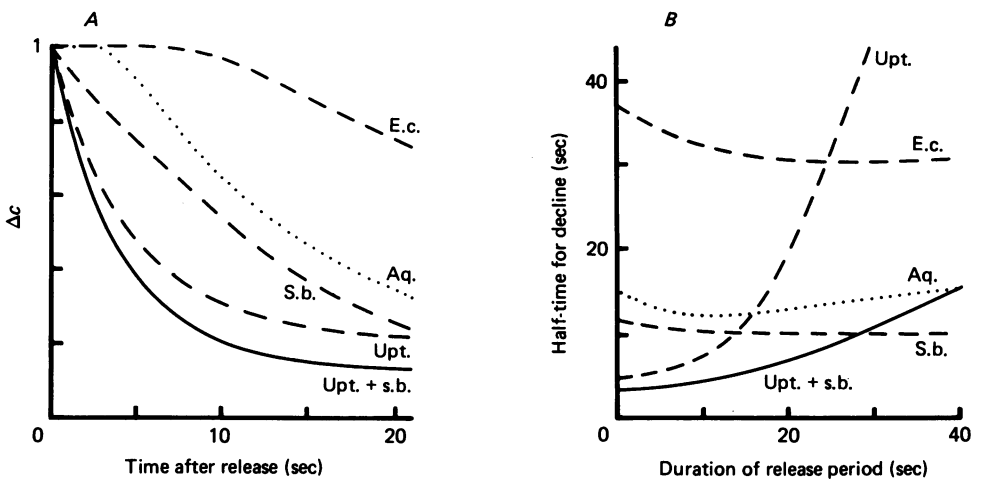

Fig. 9. Decline of $[K^+]_o$ at the centre of a release zone 0·8 mm in diameter after brief periods of release. *A*, Δc plotted against time after a sudden K^+ release. Units: fraction of the initial rise. *B*, half-time for decline of Δc as a function of the duration of a preceding period with a steady release rate. Aq.: decline expected through diffusion in an unrestricted aqueous medium with the same initial concentration distribution ($D = 2{\cdot}5 \times 10^{-5}$ cm sec^{-1}). Labels and conditions otherwise as for Fig. 7.

sole fate of K^+ is dispersal by extracellular diffusion into the surrounding tissue (e.c.), the decline at the centre over the first ten seconds is negligible (3%). With the combined buffering processes (s.b. + upt.) decline is rapid ($t_{\frac{1}{2}} = 3{\cdot}4$ sec). Each mechanism on its own (s.b. or upt.) hastens the decline considerably, with the predominant effect due to cytoplasmic uptake (upt.). It is perhaps remarkable that the spatial buffer mechanism, a passive dispersal process, can be responsible on its own for an initial drop in concentration that is orders of magnitude faster than with unrestricted aqueous diffusion (aq.). This is because initially a diffusion flux occurs only at the boundary of the release zone, while fluxes due to the electrically mediated spatial buffer action occur everywhere within a few space constants of the boundary.

The relative contributions to the decline of $[K^+]_o$ made by cytoplasmic uptake and by spatial buffer action depend on the duration of the release period. This is illustrated in Fig. 9*B* where the time for decline to half maximum of the concentration rise ($t_{\frac{1}{2}}$) is plotted as a function of the duration of a preceeding period of steady K^+ release. The values on the left-hand axis (for instantaneous release) correspond to the results of Fig. 9*A*. There is only a small dependence of $t_{\frac{1}{2}}$ on source duration with extracellular dispersal alone (e.c.) and with spatial buffer action (s.b.). With uptake, however, there is a marked increased of $t_{\frac{1}{2}}$ with increasing source duration up to 40 sec, by a factor of 4·5 when spatial buffering and uptake are combined (s.b. + upt.). This is due to the tendency of the cytoplasm (except that of the active neurones) to become fully equilibrated with raised $[K^+]_o$ during a period with prolonged K^+ release. There is little further capacity for uptake after the end of the disturbance and $[K^+]_o$ decline is prolonged by release of the cytoplasmic K^+ load instead of being hastened by uptake. This corresponds to an increase in the relative size of the slow tail of the decline, evident even for instantaneous release in Fig. 9*A* (upt. and s.b. + upt.) and illustrated further in Fig. 10*A* and *B*. The effect suggests a new explanation for the prolongation of the decline of $[K^+]_o$ after prolonged stimulation observed by Cordingley & Somjen (1978) in the cat spinal cord.

The time course of decline depends critically in many of these circumstances on τ_{eq}, which is the time constant for equilibration of cytoplasmic $[K^+]$ after a sudden change of $[K^+]_o$ to a new fixed level. The value of τ_{eq} in these calculations ($\tau_{eq} = 0{\cdot}1T = 22$ sec) is only a rough estimate since clear-cut measurements are not available. When the extracellular concentration is not fixed, and the extracellular space is itself depleted of K^+ by flux into the cytoplasm, a simple consideration of the rates of change in the two compartments shows that the time constant for equilibration is α/ξ times as great, or 4·4 sec in these calculations. Indirect arguments suggest that this is the correct order of magnitude (Gardner-Medwin, 1980). Direct equilibration between extracellular space and cytoplasm is the dominant factor in K^+ dynamics immediately after widespread and brief K^+ release (Fig. 9*A*), when the initial $[K^+]_o$ decline reflects this time constant fairly directly. On this basis the data of Vern, Schuette & Thibault (1977) and of Cordingley & Somjen (1978), giving $t_{\frac{1}{2}} = 0{\cdot}6 - 1{\cdot}5$ sec after brief stimulation periods, suggest that $\alpha\xi^{-1}\tau_{eq}$ may be somewhat less than assumed here, *ca.* 1–2 sec. However, the brief time constant in these experiments may be partly due, as suggested by the authors, to rapid K^+ re-uptake into the active neurons.

The preceding calculations have been made for K^+ release without re-uptake. When

release is due to neuronal activity it must be followed by re-uptake, though the time course of this is uncertain (p. 421). For illustration here (Fig. 10) calculations are based on an exponential model of re-uptake with a time constant of 22 sec ($0{\cdot}1T$). Re-uptake is assumed to commence even before the end of a period of stimulation. On the assumption that passive K^+ efflux occurs at a constant rate by Na/K exchange during

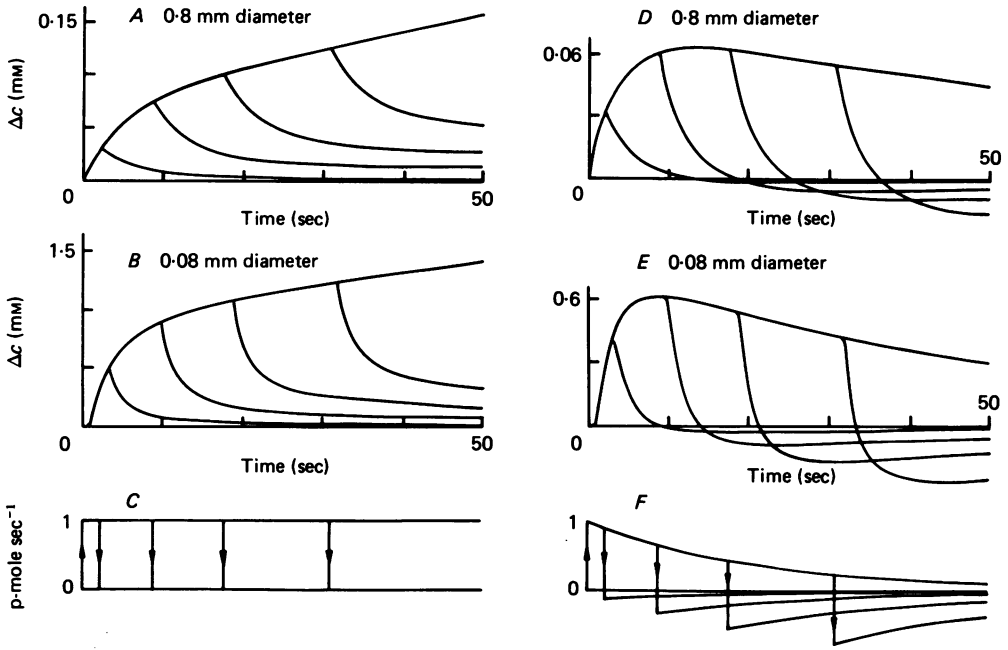

Fig. 10. Effects of K^+ re-uptake on the time course of $[K^+]_o$ changes during periods with simulated neuronal activation. Time courses of Δc for periods of steady release: on the left without re-uptake and on the right with re-uptake having an exponential time course with a time constant of 22 sec ($= 0{\cdot}1\ T$). *A* and *D* are calculated for the centre of a 0·8 mm diameter release zone. *B* and *E* are for a site 0·1 mm from the centre of a 0·08 mm diameter release zone. The time course of net release is shown in *C* and *F*. Conditions and parameters (see Fig. 7) are for spatial buffer and cytoplasmic uptake conditions together. Units: mM for a total initial release rate of 1 p-mole sec^{-1}.

stimulation and that re-uptake is proportional to Na^+ gain within the active cells, both the net efflux during stimulation and the net influx afterwards are exponentially declining functions (Fig. 10*F*). With these assumptions the time course of Δc is shown in Fig. 10*D* for the centre of a 0·8 mm diameter zone with uniform activity and in Fig. 10*E* for a site 100 μm from the centre of a 0·08 mm diameter source. The calculations assume both uptake and spatial buffering processes with the usual parameters. For comparison, Δc is shown in Fig. 10*A* and *B* without re-uptake under the same conditions. The time course of Δc after the end of stimulation exhibits an undershoot when there is re-uptake, as observed experimentally in many situations and generally attributed to re-uptake (Somjen, 1979). $[K^+]_o$ may in some conditions decline during the period of stimulation itself when there is re-uptake. These features in the calculated results are more prominent than in most experimental records of $[K^+]_o$ during stimulation (e.g. Krnjevic & Morris, 1972; Lux & Neher, 1973;

Heinemann & Lux, 1975; Kriz, Sykova & Vyklicky, 1975). The recordings are generally intermediate in shape between the right and the left sides of Fig. 10, which are calculated with and without re-uptake at the specified rate. Thus the actual re-uptake rate is probably slower than that assumed in these calculations, with a time constant greater than 22 sec.

General K^+ disturbances: spatial and temperal frequency components

The treatment of disturbances with a complex spatial and temporal pattern can be simplified by treating them as a superposition of components with different spatial and temporal frequencies. With small disturbances the equations governing the evolution of $[K^+]_o$ are linear differential equations (eqns. (15) and (22)) and the solutions are the sum of the solutions that the equations would have for the individual sinusoidal components. These sinusoidal solutions are themselves relatively simple and can be derived without numerical computations.

If the disturbance of $[K^+]_o$ from its resting level (c_B) has a sinusoidal distribution through the tissue with wavelength X, and there are no extrinsic K^+ sources (Q), then the solution to eqns. (15) and (22) corresponds to an exponential decline of the amplitude of the sinusoidal disturbance with no change of shape, wave-length or phase. Without spatial buffering ($\beta = 0$) the time constant of decline is $\xi\lambda^2X^2/(4\pi^2\alpha D)$ which, with the usual assumptions, is *ca.* 140 sec for a wave-length of 1 mm and is proportional to the square of the wave-length. If the spatial buffer mechanism is acting as well as diffusion ($\beta > 0$) then the time constant for decline is given by:

$$\tau_{\text{decline}} = \frac{\xi\lambda^2X^2}{4\pi^2\alpha D}\left(\frac{1+4\pi^2\Lambda^2/X^2}{1+\beta+4\pi^2\Lambda^2/X^2}\right). \tag{31}$$

With $\beta = 5$ and a wave-length of 1 mm, this becomes 48 sec. The ratio of the time constant with and without spatial buffering (i.e. the factor in brackets in eqn. (31)) approaches 1 for very short wave-lengths ($X \to 0$) and approaches $(1+\beta)^{-1}$ for disturbances of very long wave-lengths ($X \to \infty$). The effect of dispersal by the spatial buffer mechanism is therefore negligible by comparison with diffusion for disturbances of short wave-length and is equivalent to increasing the diffusion coefficient by a factor of about 6 ($= \beta+1$) for long wave-lengths. This same conclusion can be shown if, instead of considering the exponential decline of concentration disturbances, one considers the amplitude of a source distribution $Q(x)$ that would be required to maintain a steady sinusoidal concentration disturbance in the tissue: this is $(\beta+1)$ times greater for long wave-length disturbances and no different for short wave-lengths. The wave-length for which the speed of decline or the required source densities are doubled, with $\beta = 5$, is given by $X = \pi\Lambda$: *ca.* 0·63 mm in the rat brain.

Fluctuating source distributions $Q(x, t)$ can be analysed into components that are sinusoidal in both space and time. These yield concentration disturbances that are also sinusoidal, with phase shifts in time but not space. From eqns. (15), (28) and (29) an expression can be derived for the peak amplitude of Δc for a specified amplitude of Q, spatial frequency ($k/2\pi$) and temporal frequency ($\omega/2\pi$):

$$\Delta c_{\max} = \frac{Q_{\max}}{\alpha}\left(\frac{1+(\omega\tau_{\text{eq}})^2}{(U-\omega^2\tau_{\text{eq}})^2+\omega^2(U\tau_{\text{eq}}+\xi/\alpha)^2}\right)^{\frac{1}{2}}, \tag{32}$$

where

$$U = D\lambda^{-2}k^2(1+\beta(1+k^2\Lambda^2)^{-1}).$$

TABLE 1. Concentration changes due to sinusoidal sources. Equation (32) was used to calculate $\Delta C_{max}/Q_{max}$ for sinusoidal source distributions with wave-lengths 0·01–100 mm ($k = 630$–$0{\cdot}063$ mm^{-1}) and periods 1–10^5 sec ($\omega = 6{\cdot}3$–$6{\cdot}3 \times 10^{-5}$ sec^{-1}). Panel (*a*) shows $\Delta C_{max}/Q_{max}$ on the assumption that there is only extracellular (e.c.) dispersal ($\xi/\alpha = 1$; $\beta = 0$; $\alpha = 0{\cdot}2$; $D\lambda^{-2} = 0{\cdot}9 \times 10^{-9}$ m^2 sec^{-1}). Units are in mM for $Q_{max} = 1$ μmole l.$^{-1}$ sec^{-1}. Panels (*b*)–(*d*) show the percentage by which $\Delta C_{max}/Q_{max}$ is less than the figures in (*a*) when buffering is assumed to occur through: (*b*) cytoplasmic uptake (upt.); (*c*) spatial buffering (s.b.); (*d*) both mechanisms combined (s.b. + upt.). Parameters assumed for the buffering mechanisms are: $\xi/\alpha = 5$; $\beta = 5$; $\tau_{eq} = 22$ sec; $\Lambda = 0{\cdot}2$ mm. Dashes indicate reductions less than 0·5 %. Sectors of the Table where the reductions are greater than 50 % are marked off with lines

(*a*) $\Delta C_{max}/Q_{max}$ (e.c. dispersal)

Period (sec)	Wave-length (mm) 0·01	0·1	1	10	100
1	0·00001	0·0007	0·0008	0·0008	0·0008
10	0·00001	0·0014	0·008	0·008	0·008
100	0·00001	0·0014	0·07	0·08	0·08
10^3	0·00001	0·0014	0·14	0·8	0·8
10^4	0·00001	0·0014	0·14	7	8
10^5	0·00001	0·0014	0·14	13	79

(*b*) % reduction (upt.)

Period (sec)	Wave-length (mm) 0·01	0·1	1	10	100
1	—	1	—	—	—
10	—	5	7	6	6
100	—	3	66	67	67
10^3	—	—	27	80	80
10^4	—	—	1	77	80
10^5	—	—	—	24	80

(*c*) % reduction (s.b.)

Period (sec)	Wave-length (mm) 0·01	0·1	1	10	100
1	—	1	—	—	—
10	—	3	1	—	—
100	—	3	41	—	—
10^3	—	3	66	5	—
10^4	—	3	66	67	—
10^5	—	3	66	83	5

(*d*) % reduction (s.b. + upt.)

Period (sec)	Wave-length (mm) 0·01	0·1	1	10	100
1	—	2	—	—	—
10	—	8	10	6	6
100	—	6	73	67	67
10^3	—	3	68	80	80
10^4	—	3	66	81	80
10^5	—	3	66	83	80

Equation (32) has been evaluated (Table 1) for a range of frequencies with purely extracellular dispersal ($\beta = 0$, $\xi/\alpha = 1$) and with the usual parameters for uptake and spatial buffering (p. 414). Panel (*a*) of Table 1 gives the figures for extracellular dispersal and the remaining panels (*b*)–(*d*) give the percentages by which these figures are reduced with the buffering actions. These percentage reductions show the effectiveness of the buffer mechanisms in minimizing disturbances of $[K^+]_o$. The benefits obtained with the two separate mechanisms (s.b. and upt.) occur largely in complementary sectors of the frequency table and when combined (s.b. + upt.) they account for more than a 50 % reduction for all disturbances with a wave-length greater than *ca.* 0·6 mm and a period greater than *ca.* 50 sec. Disturbances with a smaller wave-length or a shorter period are relatively little affected by the buffering processes. Panel (*a*) in the Table shows, however, that these are disturbances in which, for a given maximal release rate Q_{max}, the concentration changes are in any case relatively small.

The buffering contribution of cytoplasmic uptake (Table 1 (*b*)), is limited at high temporal frequencies by the requirement that there be time for substantial cyto-

plasmic equilibration. It is limited also at low frequencies because the build-up of K^+ is then so prolonged that its maximum level is set by the extracellular concentration gradients that develop, driving a K^+ flux through the tissue to balance the release. Spatial buffer action (Table 1 (*c*)) is one of the mechanisms contributing to such flux. Its full effect requires wave-lengths substantially greater than the space constant (Λ) of the cells involved, but not so great that the concentration gradients become negligible. The range of wave-lengths and periods that are effectively buffered by the two mechanisms in combination is limited by Λ and by τ_{eq}. Smaller values of each of these parameters would extend the range, requiring more ion channels (or pumps) in the membranes involved than are assumed in these calculations. At present we know too little about the amplitude, distribution and frequency of normal source patterns in the nervous system or about the sensitivity of the nervous system to $[K^+]_o$ disturbances to say whether the actual frequency domains over which buffering is effective correspond to those in which there is a need for buffering.

DISCUSSION

Potassium disturbances in neural tissue are affected by factors that are hard to study experimentally in isolation. This work has attempted to identify with theoretical analysis the circumstances in which different factors are dominant, how their properties can be assessed, and the extent to which they are likely to influence normal K^+ disturbances.

The principal conclusions are that K^+ transfer through cells and K^+ equilibration with the cytoplasm of cells other than active neurones are critical factors in many experimental situations, both in the accompanying papers and in other work. These processes act to buffer changes of $[K^+]_o$ under a variety of circumstances likely to be of normal physiological importance. The ion movements involved in these mechanisms may be largely or entirely passive. These factors have probably been underestimated in recent work on K^+ dynamics (see Somjen, 1979 for review).

Re-uptake of K^+ into active neurones

The rapid build-up of $[K^+]_o$ to a plateau during stimulation of central nervous tissue and its decline afterwards with a time course of only a few seconds has been cited as evidence in favour of rapid re-uptake of K^+ by central neurones (Vern *et al.* 1977; Cordingley & Somjen, 1978). It is shown here (pp. 415–419) that such results may be due to the buffering processes discussed below rather than to re-uptake. Indeed the relatively small size of undershoots of $[K^+]_o$ normally observed experimentally after the end of stimulation suggests a re-uptake time constant substantially greater than 20 sec (p. 419). This would be more in line with the time course of metabolic changes in intact brain after neuronal activity (Lewis & Schuette, 1975; Lothman, LaManna, Cordingley, Rosenthal & Somjen, 1975).

Net uptake into cells other than active neurones

A movement of K^+ will occur into the cytoplasm of most cells that experience a rise of $[K^+]_o$ (p. 395). The experiments of Gardner-Medwin (1983) and Gardner-Medwin

& Nicholson (1983) were designed to measure K^+ transfer characteristics rather than cytoplasmic uptake. Nevertheless, while the amplitude of measured fluxes, concentration changes and voltage changes depend on the transfer parameters, the time course of their development depends also, according to the calculations based on the tissue model (Figs. 2–4), on the effective K^+ distribution space ξ defined on p. 395. A value $\xi = 1$ was found to give good agreement with the data, as illustrated in the experimental papers. Without uptake ($\xi = \alpha = 0{\cdot}2$: p. 395) the fluxes produced by current and the voltage changes produced by superfusion (Figs. 4 and 6 in Gardner-Medwin, 1983) should be expected to have developed 5 times faster than observed and the $[K^+]_o$ changes due to current flow, which at most depths did not reach a steady state (Fig. 5 in Gardner-Medwin & Nicholson, 1983), should have been up to 5 times larger than observed. It is concluded that either ξ is close to 1·0 under the condition of these experiments or else the model that forms the basis for interpretation must be seriously in error. Some inadequacy in relation to uptake must indeed be anticipated since the model assumes a strictly linear relation between tissue K^+ content and $[K^+]_o$ (i.e. ξ independent of Δc). This relation is supported for increases of $[K^+]_o$ by the data of Lund-Andersen & Hertz (1970), but with decreases of $[K^+]_o$ it must break down eventually because of diminished Na–K pumping. An extreme fall in $[K^+]_o$ from 3 mM to zero would presumably stop pumping and cause cell swelling and extreme sodium loading and a depletion of nearly all tissue potassium, amounting to 70–100 m-mole/kg ($\xi = 23$–33) before a steady state was achieved. These non-linear consequences of $[K^+]_o$ falls may explain the discrepancies between observed and expected data with such falls (Gardner-Medwin, 1983: Figs. 3 and 6). They are sufficiently uncertain that no attempt has been made to model them.

Since cytoplasmic equilibration lags somewhat behind changes of $[K^+]_o$, the time course of equilibration is sometimes important. The time constant of the lag ($\alpha\xi^{-1}\tau_{eq}$: p. 417) is probably only a few seconds, for at least a substantial fraction of the uptake (Gardner-Medwin, 1980). This lag would have a negligible effect on the prolonged time course of data obtained in the transfer experiments. The lag is not easily measured directly since sufficiently fast $[K^+]_o$ changes cannot be induced in completely controlled circumstances. A lag of 1–2 sec (corresponding to τ_{eq} = 5–10 sec) could satisfactorily account for published data on the time course of $[K^+]_o$ decline after stimulation (p. 417) and K^+ build-up close to a point source (Fig. 6). This would be consistent with other indirect data (Gardner-Medwin, 1980). Slower equilibration ($\alpha\xi^{-1}\tau_{eq} = 4{\cdot}4$ sec; $\tau_{eq} = 22$ sec) is assumed in most of the calculations here, to give cautious estimates of the buffering effects of cytoplasmic uptake (pp. 414–421).

Dispersal by diffusion and spatial buffer transfer

Spatial buffer transfer exceeds extracellular diffusion flux of K^+ in widespread disturbances of $[K^+]_o$ (pp. 410, 414, 419). With local disturbances, diffusion is dominant. The factor by which total dispersal flux is greater than diffusion flux ($\beta+1$ in the limit of low spatial frequencies) is determined by the relative resistances and K^+ transport numbers for current pathways through the transfer cells and the extracellular space. This factor was estimated by Gardner-Medwin (1983), using measure-

ments of flux across the brain surface, to be *ca.* 5·0 for the aggregate of transfer through all types of cells within rat neocortex. Calculations based on the model presented here (pp. 406–409) suggest that this estimate was low by about 15% and that the data are best fitted with $\beta + 1 = 6$ (see also Discussion of Gardner-Medwin (1983)).

The critical wave-length above which spatial buffer transfer is expected to contribute a flux greater than that due to diffusion (*ca.* 0·63 mm for rat brain: p. 419) depends also on the electrotonic space constant for the transfer cell network. The lower the membrane resistance and the greater the membrane area per unit volume of tissue the smaller is this critical wave-length. The space constant can be deduced most directly from the distribution of $[K^+]_o$ changes during current flow (Gardner-Medwin & Nicholson, 1983 and Fig. 2*C*) and is *ca.* 0·2 mm for rat cerebellar cortex. This is consistent with the inference made by Somjen & Trachtenberg (1979) that the space constant for the glial cell network must be substantially shorter than *ca.* 1 mm to account for the similarity of distribution of extracellular negativity and $[K^+]_o$ changes over such distances.

The identity of the cells involved in K^+ transfer is uncertain, though glial cells probably play a major role (Gardner-Medwin & Nicholson, 1983). We can estimate the resistance of the cytoplasmic network (r_i) and the specific membrane resistance (R_m) that would be required to give the observed transfer parameters. The expression for β (p. 399) allows us to infer that $r_i/r_o \simeq 15$. Assuming that the tortuosity of the network is the same as that of extracellular space it follows that the product (volume × conductivity) is 15 times less for pathways through the transfer cell cytoplasm and intercellular junctions than for extracellular space. We cannot infer to what extent this is due to a restricted volume fraction (α_i) or to a low internal conductivity such as might result if there are high resistance intercellular junctions (p. 397). If we assume a negligible coupling resistance and that the specific conductance of the cytoplasm is not greater than that of extracellular fluid, we can derive a minimum plausible value for the volume fraction of the transfer cells: $\alpha_i = \alpha/15 \simeq 0{\cdot}013$.

The expression for Λ given on p. 399 can be rearranged to calculate R_m:

$$R_m = \frac{\Lambda^2}{\beta} a r_o \left(\frac{1}{n_B} - 1\right). \tag{33}$$

Putting $r_o = 625\ \Omega$ cm (Gardner-Medwin, 1980) and assuming a surface to volume ratio for the transfer cells (a/α_i) of 5 μm^{-1}, equal to the average for cerebral cortex as a whole (Horstmann & Meves, 1959), we obtain $R_m = 0{\cdot}21\ \alpha_i\ M\Omega\ cm^2$. Using the lower limit for α_i derived above (0·013) we obtain $R_m \geqslant 2{\cdot}7\ k\Omega\ cm^2$. Trachtenberg & Pollen (1970) and Glötzner (1973) have measured the input time constant of mammalian glial cell networks with current injection through an intraglial microelectrode and have attempted to infer R_m for glial membranes by assuming that the input time constant is approximately equal to the membrane time constant (τ_m). This gives $R_m = 0{\cdot}2$–$0{\cdot}6\ k\Omega\ cm^2$, less than the range deduced above for the transfer cells. These figures must again be considered lower bound estimates, however, since the input time constant of a three-dimensional network is in general less than τ_m by a factor that may be large if the macroscopic network space constant is much greater

than the dimensions of an electrode or of individual network branches (Jack *et al.* 1975; chap. 5). A quantitative study of glial morphology would be required to ascertain whether the electrical input parameters of glial cells are consistent with the properties deduced for the transfer cells. If the internal network resistance is largely determined by intercellular junctions the transfer cells must be presumed to occupy more than 0·013 of the tissue and R_m might be much higher than the minimum figure calculated above: for example $R_m = 41$ kΩ cm^2 with $\alpha_i = 0{\cdot}2$.

The ratio of intracellular to extracellular potential shifts during widespread K^+ build-up is dependent largely on the ratio of intracellular and extracellular resistances, as pointed out by R. Joyner & G. Somjen (Appendix to Somjen (1973)). From eqns. (1), (3) and (4) in the present model $\Delta V_i/\Delta V_o$ is equal to $(-r_i/r_o)$, inferred above to be -15 for rat cortex. Somjen (1975: Fig. 6) estimated this quotient for cat cortex as -5, using extracellular data and indirect assumptions about the glial membrane potential changes. In the light of more recent evidence that mammalian glial cells probably show a full Nernst slope for the K^+ dependence of V_m (Somjen, 1979) the estimate by this method needs to be revised to -9. This is still less than the value (-15) expected from the K^+ transfer data in rat cortex. The discrepancy may be due either to a difference between species or to factors not included in the present model. Lothman & Somjen (1975) found an even smaller value of $\Delta V_i/\Delta V_o$ in cat spinal cord (*ca.* -2). This may indicate that the maximum ratio of spatial buffer transfer of K^+ to diffusion flux (β) is substantially greater in spinal cord than in brain.

The fate of K^+ released for long periods over a widespread zone is, according to the calculations, eventually dominated by spatial buffer transfer (Fig. 7). Somjen & Trachtenberg (1979) have estimated the extracellular and glial currents associated with spatial buffer transfer in cat spinal cord, with K^+ release over a zone *ca.* 1 mm across. The original calculation omitted a factor of 10^3 and suggested a negligible K^+ transfer; but after correction (Somjen, 1981) calculations for typical data show an excess extracellular K^+ load of $6{\cdot}0$–$7{\cdot}5 \times 10^{-10}$ mole per mm^3 of tissue to be associated with current-mediated K^+ transfer of the order of 10^{-10} mole sec^{-1} mm^{-2} across the boundary of the affected zone. The published data are from single electrode tracks; but assuming the affected zone to be roughly spherical with a diameter of 1 mm (cf. Cordingley & Somjen, 1978: Fig. 4) this would correspond to an average half time for clearance of extracellular K^+ of *ca.* 1 sec, compared with typical experimental values of 0·5–2·0 sec for the decline of $[K^+]_o$. Spatial buffer transfer may therefore be a substantial factor in K^+ clearance during widespread neuronal activation in the spinal cord. This conclusion is similar to that reached for K^+ clearance through glial cells in the isolated cut retina of the honeybee drone (Gardner-Medwin *et al.* 1981).

I thank J. A. Coles, C. Nicholson and S. Poitry for comments on this manuscript and R. K. Orkand, G. G. Somjen and C. M. Tang for helpful discussions. Much of the work was carried out while I held a Nuffield Foundation Research Fellowship.

REFERENCES

BENNETT, M. V. L. (1969). Electrical impedance of brain surfaces. *Brain Res.* **15**, 584–590.

BOCKRIS, J. O. & REDDY, A. K. N. (1970). *Modern Electrochemistry*. New York: Plenum.

BOYLE, P. J. & CONWAY, E. J. (1941). Potassium accumulation in muscle and associated changes. *J. Physiol.* **100**, 1–63.

CARSLAW, H. S. & JAEGER, J. C. (1959). *Conduction of Heat in Solids*. New York: Oxford University Press.

COHEN, L. B. & DE WEER, P. (1977). Structural and metabolic processes directly related to action potential propagation. In *Handbook of Physiology*, section 1. *The Nervous System*. vol. 1, part 1, ed. BROOKHART, J. M., MOUNTCASTLE, V. B., KANDEL, E. R. & GEIGER, S. R., pp. 137–159. Baltimore: Williams & Wilkins Co.

COLES, J. A. & TSACOPOULOS, M. (1979). Potassium activity in photoreceptors, glial cells and extracellular space in the drone retina: changes during photostimulation. *J. Physiol.* **290**, 525–549.

CONWAY, B. E. (1952). *Electrochemical Data*. Amsterdam: Elsevier.

CORDINGLEY, G. E. & SOMJEN, G. G. (1978). The clearing of excess potassium from extracellular space in spinal cord and cerebral cortex. *Brain Res.* **151**, 291–306.

DIETZEL, I., HEINEMANN, U., HOFMEIER, G. & LUX, H. D. (1980). Transient changes in the size of the extracellular space in the sensorimotor cortex of cats in relation to stimulus-induced changes in potassium concentration. *Exp. Brain Res.* **40**, 432–439.

FENSTERMACHER, J. D., PATLAK, C. S. & BLASBERG, R. G. (1974). Transport of material between brain extracellular fluid, brain cells and blood. *Fedn Proc.* **33**, 2070–2079.

FISHER, R. S., PEDLEY, T. A. & PRINCE, D. A. (1976). Kinetics of potassium movement in normal cortex. *Brain Res.* **36**, 416–419.

GARDNER-MEDWIN, A. R. (1980). Membrane transport and solute migration affecting the brain cell microenvironment. *Neurosci. Res. Progr. Bull.* **18**, 208–226.

GARDNER-MEDWIN, A. R. (1981*a*). Possible roles of vertebrate neuroglia in potassium dynamics, spreading depression and migraine. *J. exp. Biol.* **95**, 111–127.

GARDNER-MEDWIN, A. R. (1981*b*). The role of cells in the dispersal of brain extracellular potassium. In *Ion-selective Electrodes and their Use in Excitable Tissues* (ed. SYKOVA, E., HNIK, P. & VYKLICKY, L., pp. 339–343. New York: Plenum.

GARDNER-MEDWIN, A. R. (1983). A study of the mechanisms by which potassium moves through brain tissue in the rat. *J. Physiol.* **335**, 353–374.

GARDNER-MEDWIN, A. R., COLES, J. A. & TSACOPOULOS, M. (1981). Clearance of extracellular potassium: evidence for spatial buffering by glial cells in the retina of the drone. *Brain Res.* **209**, 452–457.

GARDNER-MEDWIN, A. R., GIBSON, J. & WILLSHAW, D. J. (1979). The mechanism of potassium dispersal in brain tissue *J. Physiol.* **293**, 37–38*P*.

GARDNER-MEDWIN, A. R. & NICHOLSON, C. (1983). Changes of extracellular potassium activity induced by electric current through brain tissues in the rat. *J. Physiol.* **335**, 375–392.

GLÖTZNER, F. L. (1973). Membrane properties of neuroglia in epileptogenic gliosis. *Brain Res.* **55**, 159–171.

GOLDMAN, D. E. (1943). Potential, impedance and rectification in membranes. *J. gen. Physiol.* **27**, 37–60.

HEINEMANN, U. & LUX, H. D. (1975). Undershoots following stimulus induced rises of extracellular potassium concentration in cerebral cortex of cat. *Brain Res.* **93**, 63–76.

HORSTMANN, E. & MEVES, H. (1959). Die Feinstruktur des molekularer Rindengraues und ihre physiologische Bedeutung. *Z. Zellforsch. mikrosk. Anat.* **49**, 569–604.

JACK, J. J. B., NOBLE, D. & TSIEN, R. W. (1975). *Electric Current Flow in Excitable Cells*. Oxford: Clarendon.

KATZMAN, R. & LEIDERMAN, P. H. (1953). Brain potassium exchange in normal adult and immature rats. *Am. J. Physiol.* **175**, 263–270.

KŘÍŽ, N., SYKOVÁ, E. & VYKLICKÝ, L. (1975). Extracellular potassium changes in the spinal cord of the cat and their relation to slow potentials, active transport and impulse transmission. *J. Physiol.* **249**, 167–182.

KRNJEVIĆ, K. & MORRIS, M. E. (1972). Extracellular K^+ activity and slow potential changes in spinal cord and medulla. *Can. J. Physiol. Pharmac.* **50**, 1214–1217.

LEVIN, V. A., FENSTERMACHER, J. D. & PATLAK, C. S. (1970). Sucrose and inulin space measurements of cerebral cortex in four mammalian species. *Am. J. Physiol.* **219**, 1528–1533.

LEWIS, D. V. & SCHUETTE, W. H. (1975). NADH fluorescence and $[K^+]_o$ changes during hippocampal electrical stimulation. *J. Neurophysiol.* **38**, 405–417.

LOTHMAN, E. W., LA MANNA, J., CORDINGLEY, G., ROSENTHAL, M. & SOMJEN, G. G. (1975). Responses of electrical potential, potassium levels, and oxidative metabolic activity of cerebral neocortex of cats. *Brain Res.* **88**, 15–36.

LOTHMAN, E. W. & SOMJEN, G. G. (1975). Extracellular potassium activity, intracellular and extracellular potential responses in the spinal cord. *J. Physiol.* **252**, 115–136.

LUND-ANDERSEN, H. & HERTZ, L. (1970). Effects of potassium and of glutamate on swelling and on sodium and potassium content of brain-cortex slices from adult rats. *Exp. Brain Res.* **11**, 199–212.

LUX, H. D. & NEHER, E. (1973). The equilibration time course of $[K^+]_o$ in cat cortex. *Exp. Brain Res.* **17**, 190–205.

NICHOLSON, C. & PHILLIPS, J. M. (1981). Ion diffusion modified by tortuosity and volume fraction in the extracellular microenvironment of the rat cerebellum. *J. Physiol.* **321**, 225–257.

NICHOLSON, C., PHILLIPS, J. M. & GARDNER-MEDWIN, A. R. (1979). Diffusion from an ionophoretic point source in the brain: role of tortuosity and volume fraction. *Brain Res.* **169**, 580–584.

ORKAND, R. K., NICHOLLS, J. G. & KUFFLER, S. W. (1966). Effect of nerve impulses on the membrane potential of glial cells in the central nervous system of amphibia. *J. Neurophysiol.* **29**, 788–806.

SOMJEN, G. G. (1973). Electrogenesis of sustained potentials. *Prog. Neurobiol.* **1**, 199–237.

SOMJEN, G. G. (1975). Electrophysiology of neuroglia. *A. Rev. Physiol.* **37**, 163–190.

SOMJEN, G. G. (1979). Extracellular potassium in the mammalian central nervous system. *A. Rev. Physiol.* **41**, 159–177.

SOMJEN, G. G. (1981). The why and how of measuring the activity of ions in extracellular fluid of spinal cord and cerebral cortex. In *The Application of Ion-selective Electrodes*, ed. ZEUTHEN, T., pp. 175–193. Amsterdam: Elsevier.

SOMJEN, G. G. & TRACHTENBERG, M. (1979). Neuroglia as generator of extracellular current. In *Origin of Cerebral Field Potentials*, ed. SPECKMANN, E. J. & CASPERS, H., pp. 21–32. Stuttgart: Georg Thieme.

TRACHTENBERG, M. C. & POLLEN, D. A. (1970). Neuroglia: biophysical properties and physiologic function *Science, N.Y.* **167**, 1248–1252.

VARON, S. S. & SOMJEN, G. G. (1979). Neuron–glia interactions. *Neurosci. Res. Progr. Bull.* **17**, 1–239.

VERN, B. A., SCHUETTE, W. H. & THIBAULT, L. E. (1977). $[K^+]_o$ clearance in cortex: a new analytical model. *J. Neurophysiol.* **40**, 1015–1023.